Title

Auxin-salicylic acid seesaw regulates the age-dependent balance between plant growth and herbivore defense

Authors

Wen-Hao Han[1]†, Feng-Bin Zhang[1]†, Shun-Xia Ji[1], Kai-Lu Liang[1], Jun-Xia Wang[1], Xiao-Ping Fan[2], Shu-Sheng Liu[1], Xiao-Wei Wang[1]*

Affiliations

[1]State Key Laboratory of Rice Biology and Breeding, Ministry of Agriculture Key Lab of Molecular Biology of Crop Pathogens and Insects, Zhejiang Key Laboratory of Biology and Ecological Regulation of Crop Pathogens and Insects, Institute of Insect Sciences, Zhejiang University, Hangzhou 310058, China.

[2]LC-Bio Technology Co., Ltd, Hangzhou, China.

*Corresponding author. Email: xwwang@zju.edu.cn

†These authors contributed equally to this work.

Abstract

Plants must fine-tune their needs for growth and defense. According to the Plant Vigor Hypothesis, younger, more vigorous plants tend to be more susceptible to herbivores compared to older, mature plants, yet the molecular mechanisms underlying this dynamic remain elusive. Here, we uncover a hormonal crosstalk framework that orchestrates the age-related balance between plant growth and herbivore defense. We demonstrate that the accumulation of salicylic acid (SA), synthesized by *Nicotiana benthamiana* phenylalanine ammonia-lyase 6 (NbPAL6), dictates insect resistance in adult plants. The expression of *NbPAL6* is driven by the key transcription factor, NbMYB42, which is regulated by two interacting auxin response factors, NbARF18La/b. In juvenile plants, higher auxin levels activate *Nb*miR160c, a microRNA that silences *NbARF18La/b*, subsequently reducing *NbMYB42* expression, lowering SA accumulation, and thus weakening herbivore defense. Furthermore, excessive SA accumulation in juvenile plants enhances defense but antagonizes auxin signaling, impairing early growth. Our findings suggest a seesaw-like model that balances growth and herbivore defense depending on the plant's developmental stage.

Keywords

Plant age, Balance, Phytohormone cross-talk, Insect defense, Growth, MicroRNA, Auxin, Salicylic acid

Teaser

The crosstalk between two phytohormones enables plants to achieve a balance between growth and defense against insects across growth stages.

MAIN TEXT

Introduction

Plants, being sessile organisms, must constantly navigate hostile environments to survive and reproduce, facing a wide range of abiotic and biotic stresses. Over time, they have evolved sophisticated systems to detect, respond to, and defend against environmental changes. However, these defenses come at a significant cost, often resulting in trade-offs with growth and development (*1, 2*). Among the most damaging threats to plants are herbivorous insects, which can attack at any stage of plant development. While tissue-chewing insects cause direct damage by consuming plant tissues, phloem-feeding insects pierce the epidermis to delicately extract nutrient-rich phloem sap using needle-like mouthparts. In response to such threats, plants have evolved both inducible and constitutive defense mechanisms (*3, 4*). Induced defenses are triggered in response to specific stimuli, while constitutive defenses involve continuous accumulation of insecticidal components throughout the plant's growth and development (*5, 6*). Given that insect attacks are often sporadic, plants must finely balance their investment in growth with the need for defense. However, how this balance is maintained at the molecular level remains poorly understood.

In the context of plant-herbivore interactions, the Plant Vigor Hypothesis (PVH) posits that herbivores preferentially target young, vigorous plants over older, mature ones (*7, 8*). At the same time, plants tend to develop increased resistance to biological stresses, such as pathogens and herbivores, as they age—a phenomenon known as age-related resistance (ARR) (*9–13*). These observations suggest that plants may prioritize rapid growth early in life, tolerating some degree of herbivore damage, before shifting their focus to defense mechanisms later in development (*14*). However, the precise mechanisms underlying PVH and ARR in the context of herbivores remain largely unexplored. Given the dual necessity for plants to grow and defend themselves, a better understanding of how this balance is optimized holds significance to both ecological theory and agricultural production.

Phytohormones play a pivotal role in regulating various aspects of plant growth, development, and defense, often through intricate crosstalk mechanisms (*15, 16*). Auxin, the first phytohormone discovered, along with other phytohormones, orchestrates plant growth and development while also modulating stress responses (*15*). Among stress-related hormones, jasmonic acid (JA), salicylic acid (SA), abscisic acid (ABA), and ethylene (ET) are key players, particularly in response to herbivory, with JA being central to resistance against tissue-chewing insects and SA being crucial for defense against phloem-feeding insects (*14, 16*). The interaction between these phytohormones has complex effects on plants against insects (*16*). For instance, the JA-SA antagonistic relationship is a well-studied area, with each hormone modulating plant responses to different herbivores. Moreover, other phytohormones,

including auxin, ET, ABA, gibberellins (GA), brassinosteroids (BR), and cytokinins (CK) are also involved in fine-tuning plant immunity by influencing JA and SA signaling pathways, especially in response to pathogens and abiotic stresses (*16*). The intricate mechanisms of phytohormonal interplay involve multiple layers of regulation, including transcriptional control by transcription factors (TFs), post-transcriptional regulation by small RNAs (sRNAs), and control of protein activity (*17–20*). Despite these advances, it remains unclear how plants integrate hormonal signals to balance growth and defense at different developmental stages.

The whitefly, *Bemisia tabaci* (Gennadius), is a species complex, several species of which are of agricultural importance worldwide (*21–24*). A few species of this whitefly complex are highly polyphagous, exhibiting remarkable adaptability to different hosts (*25, 26*). Being phloem-feeders, whiteflies use their piercing-sucking mouthparts delicately to extract nutrients, making juvenile, vigorous plants particularly vulnerable to attacks and yield losses (*26–28*). Understanding the underlying mechanisms that govern plant growth-defense balance could be key to developing sustainable whitefly control strategies.

Nicotiana benthamiana has become an important model organism in plant molecular biology and biotechnology, serving as a bio-factory for vaccines and pharmacological compounds (*29, 30*). Our previous studies have shown that *N. benthamiana* exhibits strong attraction to and lethal effects on several Hemiptera and Thysanoptera insects, including whiteflies, winged aphids, and thrips, highlighting its potential as a dead-end trap plant for field pest control (*31–33*). However, we observed that the insecticidal efficacy of *N. benthamiana* varied with the plant's development stage. Upon further investigation, we found that beyond environmental influences, this age-related defense capacity was closely tied to the developmental stage, suggesting a complex regulatory mechanism involving ARR. These findings underscore the utility of *N. benthamiana* as a system to study ARR and provide a foundation for its application in pest management.

In this study, we demonstrate that auxin-SA crosstalk mediates the balance between plant growth and herbivore defense at different developmental stages. We reveal that the establishment of ARR in *N. benthamiana* and several other Solanaceae species is closely tied to SA levels. Using molecular biology and biochemical approaches, we elucidate that the NbARF18La/b-NbMYB42-NbPAL6 signaling module plays a critical role in the age-related regulation of SA accumulation. Furthermore, we find that the age-dependent auxin-miRNA160c module also contributes to this process. Our findings provide new insights into PVH and lay the theoretical groundwork for developing innovative pest control strategies against whiteflies.

Results

Age-regulated resistance against phloem-feeding insects in Solanaceae plants

To compare the defense levels of plants at different ages against phloem-feeding insects, we conducted bioassays of *B. tabaci* whiteflies, *Myzus persicae* aphids, and *Frankliniella occidentalis* western flower thrips on several Solanaceae species, including *N. benthamiana*, *Solanum lycopersicum* (tomato), and *Nicotiana tabacum* (tobacco). In *N. benthamiana*, both the survival rate and fecundity of whiteflies were significantly lower on adult plants (35 days old, with 8–9 true leaves) compared to juvenile plants (21 days old, with 3–4 true leaves) **(Fig. 1, A and B)**. Similarly, whiteflies performed better on juvenile tobacco (21 days old, 3–4 true leaves) and tomato (21 days old, 3–4 true leaves) plants compared to adult plants (35 days old, 6–7 true leaves for tobacco; 8–9 true leaves for tomato) **(Fig. 1, A and B)**. Additionally, western flower thrips showed higher survival rates, and aphids produced more offspring on juvenile plants compared to adult plants **(Fig. 1, C and D)**. These results demonstrate ARR against phloem-feeding insects in Solanaceae plants.

SA-dependent ARR against phloem-feeding insects

To explore the mechanism underlying ARR, we focused on *N. benthamiana,* which exhibited the most pronounced age-dependent insect resistance. We examined whether the defense phytohormones SA and JA were involved in ARR by comparing the basal levels of SA and JA in 21-day-old and 35-day-old *N. benthamiana* plants. SA levels were higher in adult plants, while JA levels showed no significant differences between juvenile and adult plants **(Fig. 1, E and F)**. This trend was also observed in tobacco **(Fig. 1, E and F)**. Additionally, the expression of *pathogenesis-related 1* (*NbPR1*), a downstream marker of SA signaling, was significantly upregulated in adult plants, indicating enhanced SA signaling **(Fig. S1A)**.

To further investigate the role of SA in ARR, we used *N. benthamiana* transgenic plants expressing the *NahG* gene, which encodes salicylate hydroxylase from *Pseudomonas putida*, an enzyme that depletes SA accumulation (*34*). Unlike wild-type plants, *NahG* plants were unable to accumulate sufficient SA as they aged **(Fig. 1G),** and the mRNA levels of *NbPR1* were also significantly reduced in 35-day-old plants **(Fig. S1B).** Moreover, whitefly infestation failed to induce SA accumulation in *NahG* plants **(Fig. 1H)**. Bioassays revealed that whiteflies performed better on both juvenile and adult NahG plants compared to wild-type plants **(Fig. 1I)**, indicating that both whitefly-inducible and growth-accumulated SA are critical for plant defense against whiteflies. Exogenous SA application further confirmed SA's role in ARR. Treatment with SA increased *NbPR1* expression and enhanced whitefly defense in 21-day-old wild-type plants **(Fig. 1J and Fig. S1C)**, as well as in 35-day-old *NahG* plants **(Fig. 1K)**. These results collectively confirm that ARR in *N. benthamiana* against whiteflies is SA-dependent.

SA-mediated ARR depends on the expression of the SA synthesis gene *NbPAL6*

In plants, SA is synthesized via two distinct pathways: the phenylalanine ammonia lyase (PAL) pathway and the isochorismate synthase (ICS) pathway (*35*) **(Fig. 2A)**. To assess whether gene expression in these pathways changes with plant age, we performed reverse transcription quantitative PCR (RT-qPCR). The results showed no significant differences in the transcript levels of *NbICS1* and *NbICS2*, or the the two TFs, *CaM-Binding Protein 60g* (*CBP60g*) and *Systemic Acquired Resistance Deficient 1* (*SARD1*), which activate the *ICS* pathway **(Fig. 2B)**. Similarly, components of the ICS pathway such as *Enhanced Disease Susceptibility 5* (*EDS5*) and *AvrPphB Susceptible 3* (*PBS3*) were downregulated with plant age, while *Enhanced Pseudomonas Susceptibility 1* (*EPS1*) remained unchanged **(Fig. 2B)**. Given these findings, we shifted our focus to the PAL pathway.

A search of the *N. benthamiana* genome database (https://www.nbenth.com/) identified nine *PAL* genes (*NbPAL1-NbPAL9*), which we classified into four phylogenetic branches, likely representing alleles from the allotetraploid ancestry of *N. benthamiana* **(Fig. S2 and Table S1)**. From these, we selected four *PAL* genes (*NbPAL4*, *NbPAL6*, *NbPAL7*, and *NbPAL9*) from the four branches respectively for further analysis. Expression profiling across developmental stages revealed that only *NbPAL6* showed increased transcription with plant age, while the other genes remained unchanged **(Fig. 2C)**.

To determine whether *NbPAL6* is involved in SA-mediated ARR, we employed virus-induced gene silencing (VIGS) and *Agrobacterium*-mediated overexpression to manipulate *NbPAL6* expression in *N. benthamiana* (*29, 36*). The timing of these treatments was carefully designed to align with plant age requirements **(Fig. 2D)**. In the VIGS system, we injected the pTRV2 vector into 21-day-old plants., which led to effective gene silencing within 14 days **(Fig. 2D)**. This period of transcriptional inhibition coincides with the establishment of ARR, making VIGS an ideal system for studying gene-related ARR **(Fig. 2D)**. Compared to control plants (injected with an empty vector), 35-day-old VIGS-treated plants showed a significant reduction in target gene transcript accumulation after reaching 21 days of age. Subsequent validation experiments on the 35-day VIGS-treated plants provide valuable insights into the role of target genes in ARR establishment. Meanwhile, *Agrobacterium*-mediated overexpression can be used to enhance the mRNA level of target genes in both 21-day-old and 35-day-old plants, enabling examination of gene function in plants of different ages **(Fig. 2D)**. We injected 19-day-old plants with the pCAMBIA1305-GFP vector containing the target gene. Two days later, during the vector's active period, elevated target gene mRNA levels were observed in the 21-day-old plant. By comparing overexpressed plants with control plants (injected with an empty vector), we could evaluate the effect of target genes on resistance in 21-day-old

plants **(Fig. 2D)**. Similarly, this method can also verify the effect of target gene overexpression in 35-day-old plants **(Fig. 2D)**.

Our results showed that 35-day-old VIGS-*NbPAL6* plants could not accumulate SA to the same levels as control (VIGS-EV) plants, nor could they upregulate *NbPR1* expression **(Fig. 2, E and F; Fig. S3A)**. Moreover, these plants exhibited reduced resistance to whiteflies **(Fig. 2G)**. Conversely, overexpression of *NbPAL6* at 21 days of age significantly increased the *NbPR1* levels and improved plant defense against whiteflies **(Fig. 2H; Fig. S3, B and C)**. These findings indicate that the differential expression of *NbPAL6* between juvenile and adult stages regulates SA level and SA-mediated ARR against whiteflies in *N. benthamiana*.

Age-regulated NbMYB42 activates *NbPAL6* transcription

To identify the upstream TFs regulating *NbPAL6* expression, we screened the *NbPAL6* promoter (*NbPAL6pro*) using a yeast one-hybrid (Y1H) system with a cDNA library from *N. benthamiana*. NbMYB42, a TF belonging to the R2R3-MYB family, was identified. R2R3-MYB is known to regulate the phenylpropanoid metabolic pathway (*37–39*). Yeast transformants containing the plasmids pAbAi-*NbPAL6pro* and pGADT7-NbMYB42 were able to grow on SD/-Leu medium with 150 ng/ml AbA within 3 days, while control transformants with pAbAi-*NbPAL6pro* and pGADT7 did not **(Fig. 3A)**. This indicates that NbMYB42 can bind to the *NbPAL6* promoter. NbMYB42 was also found to localize in the nucleus **(Fig. 3B)**, suggesting its role as a nuclear TF. To assess its role in activating *NbPAL6* expression *in vivo*, we performed the GUS staining assays. The results showed that *NbPAL6pro*::*GUS* co-infiltrated with *35S*::*NbMYB42* exhibited significantly higher GUS staining levels compared to the empty vector control in *N. benthamiana* leaves **(Fig. 3C)**. Similarly, dual-luciferase reporter assays demonstrated increased luciferase activity when *NbPAL6pro::LUC* was co-expressed with *35S::NbMYB42* **(Fig. 3D)**. These results confirmed that NbMYB42 activates *NbPAL6* promoter expression.

Next, we explored whether NbMYB42 directly binds to specific sites within the *NbPAL6pro*. Using the Jasper database (https://jaspar.elixir.no/), we identified five potential *MYB* binding sites (P1–P5) **(Fig. 3E)**. To validate binding *in vivo*, we conducted chromatin immunoprecipitation (ChIP)-qPCR using plants overexpressing *NbMYB42* with glutathione S-transferase (GST) tag. We designed primers specific to the five binding sites to assess their interaction with NbMYB42 **(Table S2)**. The experiments were carried out using an anti-GFP antibody. Binding activity was observed at P1, P3, P4, and P5, but not P2, in the immunoprecipitated chromatin, indicating significantly accumulation of NbMYB42-GFP at these sites compared to the GFP control **(Fig. 3F)**. Furthermore, electrophoretic mobility shift assay (EMSA) with recombinant NbMYB42-GST, purified from *Escherichia coli*, confirmed the binding activity *in vitro*. The MYB element site P3, which showed the strongest

243 binding ability in the ChIP-qPCR test, was selected to prepare the biotin-labeled
244 probe according to its sequence **(Table S2)**. We observed that the NbMYB42-GST
245 protein was able to bind directly to the P3 probe, while the mutated probe eliminated
246 NbMYB42-GST binding **(Fig. 3G)**. Additionally, an unlabeled P3 probe was prepared
247 as the cold competitors. With the increase of competitor probes (10, 20, and 50 ×), the
248 shifted band corresponding to the P3-probe and the NbMYB42 complex gradually
249 disappeared **(Fig. 3G)**, suggesting the binding capacity was greatly reduced by the
250 addition of unlabeled cold competition probe. These results collectively show that
251 NbMYB42 specifically binds to the MYB *cis*-element on the *NbPAL6* promoter.
252
253 We then studied whether NbMYB42 influences ARR against whiteflies by regulating
254 NbPAL6-mediated SA accumulation. Overexpressing *NbMYB42* in 21-day-old *N.*
255 *benthamiana* plants increased *NbPAL6* expression more than 150-fold compared to
256 control plants **(Fig. 3H and Fig. S4A)**. The SA-downstream *NbPR1* was also
257 significantly upregulated **(Fig. S4B)**. This overexpression enhanced whitefly
258 resistance in 21-day-old plants **(Fig. 3I)**. Conversely, silencing *NbMYB42* in 35-day-
259 old plants **(Fig. S4C)** suppressed *NbPAL6* expression **(Fig. 3J)**, resulting in reduced
260 SA and *NbPR1* levels **(Fig 3. K and L)**. Notably, the *NbMYB42*-silenced 35-day-old
261 *N. benthamiana* plant showed significantly reduced whitefly defense compared to
262 control **(Fig. 3M)**. These results indicate that NbMYB42 plays a crucial role in ARR
263 in *N. benthamiana* by regulating *NbPAL6* expression and SA accumulation.
264
265 **Two interacting age-regulated NbARFs activate the expression of *NbMYB42***
266 We observed that *NbMYB42* expression was significantly higher in 35-day-old plants
267 compared to 21-day-old plants **(Fig. 4A)**, prompting further investigation into how
268 *NbMYB42* expression is regulated during *N. benthamiana* development. Using a Y1H
269 assay, we screened for TFs that regulate *NbMYB42* expression and identified two
270 auxin response factors (ARFs) with distinct evolutionary relationships, which we
271 named NbARF18La and NbARF18Lb **(Fig. S5A)**. Yeast strains harboring the pAbAi-
272 *NbMYB42pro* and pGADT7-NbARF18La or pGADT7-NbARF18Lb constructs were
273 able to grow on SD/-Leu medium supplemented 150 ng/ml AbA, whereas yeast
274 strains containing pAbAi-*NbMYB42pro* and a control pGADT7 plasmid could not
275 **(Fig. 4B)**, suggesting that both NbARF18La and NbARF18Lb bind to the *NbMYB42*
276 promoter.
277
278 Phylogenetic analysis showed that NbARF18La and NbARF18Lb are closely related
279 to ARF16 from *Arabidopsis thaliana* **(Fig. S5A)**. Amino acid sequence analysis
280 revealed conserved B3-type DNA-binding domains in the N-termini of both
281 NbARF18La and NbARF18Lb and dimerization domains in their C- termini (*40–43*)
282 **(Fig. S5B)**. Subcellular localization analysis confirmed that both NbARFs are
283 localized in the nucleus **(Fig. 4C)**, indicating their function as nuclear TFs. To verify
284 the activation of *NbMYB42* by these NbARFs, we conducted GUS staining and dual-

285 luciferase reporter assays. Co-expression of *35S::NbARF18La* and *35S::NbARF18Lb*
286 with the reporter *NbMYB42pro::GUS* in *N. benthamiana* leaves significantly
287 increased *GUS* expression **(Fig. 4D)**, and dual-luciferase reporter assay showed a
288 significant up-regulation in LUC/REN ratio when *35S::NbARF18La* and
289 *35S::NbARF18Lb* were co-expressed with the *NbMYB42pro*::*LUC* reporter **(Fig. 4E)**.
290 These results collectively demonstrate that NbARF18La and NbARF18Lb activate
291 *NbMYB42* expression.
292
293 **DNA-binding specificity of NbARF18La and NbARF18Lb**
294 To explore how the two NbARFs specifically bind to the *NbMYB42* promoter, we
295 screened for potential auxin response elements (AuxRE) using the JASPAR database
296 and identified three regions (P1, P2, and P3) in the promoter **(Fig. 4F)**. We designed
297 primers specific to these regions **(Table S2)** and performed ChIP-qPCR using GFP-
298 tagged NbARF18La/b and anti-GFP antibodies. The results revealed a significant
299 enrichment of the P2 region, but not P1 and P3, in the immunoprecipitated chromatin,
300 indicating that *NbARF18La*/*b* bind to the P2 AuxRE region (TGTCTC) in the
301 *NbMYB42* promoter **(Fig. 4F)**.
302
303 To confirm the binding specificity, we conducted an EMSA assay. The recombinant
304 NbARF18La-His-SUMO fusion protein bound to the P2 probe of the NbMYB42
305 promoter, while no binding occurred with a mutant probe (TGTCTC to AAAAAA)
306 **(Fig. 4G)**. Additionally, competition assays using unlabeled probes verified the
307 specificity of binding **(Fig. 4G)**. Similarly, the NbARF18Lb-MBP fusion protein
308 bound to the same promoter region (P2), but not to the mutant probe, and competition
309 with unlabeled probes also reduced the binding strength **(Fig. 4H)**. Together, these
310 results indicate that NbARF18La and NbARF18Lb specifically bind to the same
311 AuxRE site in the *NbMYB42* promoter.
312
313 **NbARF18La and NbARF18Lb interaction and self-association**
314 Previous studies have shown that ARF TFs can form complexes through self-
315 interactions or by interacting with other TFs (*41–44*). To explore potential interactions
316 between *NbARF18La* and *NbARF18Lb* or self-interactions of either of the TFs, we
317 performed yeast two-hybrid (Y2H) assays. Yeast cells expressing NbARF18La-
318 AD/NbARF18Lb-BD grew on selective selective media (SD/-Leu-Trp-His-Ade),
319 indicating that NbARF18La and NbARF18Lb can interact with each other **(Fig. S6A)**.
320 Additionally, NbARF18La was able to interact with itself in Y2H assays **(Fig. S6A)**.
321
322 We then confirmed these interactions *in vivo* using a bimolecular fluorescence
323 complementation (BiFC) assay. GFP fluorescence was detected in *N. benthamiana*
324 leaves co-expressing NbARF18La and NbARF18Lb or NbARF18La alone **(Fig.
325 S6B).** *In vitro* pull-down assays further validated these interactions, as His-
326 NbARF18La exhibited an affinity for MBP-NbARF18Lb, but no interaction was

327 observed in the negative control **(Fig. S6C)**. These results demonstrate that
328 NbARF18La and NbARF18Lb physically interact and NbARF18La can self-interact,
329 suggesting that these interactions are important for cooperatively regulating
330 *NbMYB42* expression.
331
332 **NbARFs regulate plant resistance to whiteflies in an age-related manner**
333 Next, we examined the role of NbARF18La and NbARF18Lb in ARR to whiteflies in
334 *N. benthamiana*. Overexpression of both NbARFs significantly upregulated
335 expression of *NbMYB42*, *NbPAL6*, and the downstream *NbPR1* gene in 21-days-old
336 plants **(Fig. 5A; Fig. S7A to C)**, which led to enhanced resistance to whiteflies **(Fig.
337 5B)**. In contrast, silencing *NbARF* genes via VIGS in 35-day-old *N. benthamiana*
338 plants resulted in substantially reduced expression of *NbMYB42* and *NbPAL6* **(Fig.
339 5C; Fig. S7D and E)**, as well as significantly decreased endogenous SA levels and
340 reduced *NbPR1* expression **(Fig. 5D; Fig. S7F)**. Correspondingly, silencing *NbARFs*
341 impaired the defense response against whiteflies in adult plants **(Fig. 5E)**.
342
343 To further investigate how NbARFs regulate *NbPAL6* expression, we co-expressed
344 NbARF18La/b with a LUC reporter fused to the *NbPAL6* promoter, which
345 significantly enhanced LUC activity **(Fig. 5F)**, indicating that NbARF18La/b regulate
346 *NbPAL6* by modulating the expression of *NbMYB42*. Furthermore, expression of
347 *NbARF18La/b* was significantly higher in 35-day-old plants than in 21-day-old plants
348 **(Fig. 5G)**, indicating that the NbARF18La/b-*NbMYB42-NbPAL6* module is regulated
349 in an age-dependent manner.
350
351 **Auxin suppresses plant defense by repressing SA accumulation in juvenile plants**
352 Given the findings above, we questioned why SA-mediated defense is not fully
353 established during the juvenile stage of plants. Since defense-related ARF TFs are key
354 components downstream of the auxin response, we postulated that auxin is involved
355 in this process. To test this hypothesis, we first measured the levels of indole-3-acetic
356 acid (IAA) in 21-day-old and 35-day-old plants, and found that IAA levels were
357 significantly higher in juvenile plants **(Fig. 6A)**. In parallel, we observed elevated
358 expression levels of the auxin synthesis genes, *TRYPTOPHAN
359 AMINOTRANSFERASE RELATED 2* (*NbTAR2*) and *YUCCA 8* (*NbYUC8*), as well as
360 the auxin-responsive gene *NbIAA29*, in juvenile plants **(Fig. 6B)**.
361
362 To assess the effect of auxin on plant defense, we treated 35-day-old plants, which are
363 known for their high resistance to whiteflies, with natural IAA and the auxin-like
364 plant growth regulator, 1-naphthalene acetic acid (NAA). Bioassays revealed that the
365 whiteflies performed better on IAA- and NAA-treated plants, indicating that auxin
366 negatively impacts plant defense **(Fig. 6, C and D)**. Furthermore, IAA treatment
367 significantly suppressed both the SA level **(Fig. 6E)** and the expression of the SA-
368 responsive gene *NbPR1* **(Fig. 6F)** in the 35-day-old plants.

To further clarify the role of auxin in repressing SA-based resistance, we treated 21-day-old plants with two auxin biosynthesis inhibitors: L-kynurenine (L-Kyn), a competitive substrate inhibitor, and Yucasin (5-(4-chlorophenyl)-4H-1,2,4-triazole-3-thiol), an effective IAA biosynthesis inhibitor (*45*). Plants treated with these auxin inhibitors showed increased resistance to whiteflies **(Fig. S8, A and B)**, as well as higher expression levels of *NbPR1* **(Fig. S8C)**. These results confirm that auxin suppresses SA biosynthesis and downstream signaling pathways in juvenile *N. benthamiana* plants, thereby repressing SA-mediated defense against whiteflies.

Auxin suppresses *NbPAL6* and *NbMYB42* expression by repressing NbARF levels

To explore how auxin suppresses SA accumulation, we focused on the age-regulated SA synthesis gene *NbPAL6*. Auxin treatment significantly reduced *NbPAL6* expression in 35-day-old plants **(Fig. 6G)**, whereas treatment with an auxin inhibitor enhanced *NbPAL6* expression in 21-day-old plants **(Fig. S8D)**. To investigate the underlying mechanism, we used *NbPAL6* promoter-driven GUS and LUC reporter, which showed decreased transcript levels upon auxin treatment, indicating that auxin suppresses *NbPAL6* expression through transcriptional repression **(Fig. 6H)**.

We hypothesized that auxin may inhibit *NbPAL6* transcription by suppressing the activity of the TF *NbMYB42*. However, *NbPAL6* promoter-linked GUS and LUC reporter assays in IAA-treated plants revealed no significant impact on reporter expression **(Fig. 6I)**, suggesting that auxin does not affect the transactivation ability of *NbMYB42*.

Next, we assessed whether auxin affects *NbMYB42* mRNA levels. qRT-PCR revealed a significant reduction in *NbMYB42* mRNA levels in auxin-treated 35-day-old plants **(Fig. 6J)**, whereas auxin inhibitor treatment enhanced *NbMYB42* expression in 21-day-old plants **(Fig. S8E)**. A reporter-GUS assay further confirmed that auxin represses *NbMYB42* transcription **(Fig. 6K)**. These results indicate that auxin represses *NbMYB42* transcription, thereby regulating downstream *NbPAL6* expression.

To understand how auxin represses *NbMYB42* transcription, we examined upstream TFs, *NbARF18La* and *NbARF18Lb*. Surprisingly, auxin treatment did not affect the activation of *NbMYB42* by NbARF18La/b **(Fig. 6, L and M)**. However, auxin significantly decreased the transcript levels of *NbARF18La/b* in 35-day-old plants **(Fig. 6N)**, with auxin inhibitors increasing their expression in 21-day-old plants **(Fig. S8F)**. These results indicate that auxin downregulates *NbARF18La/b*, which in turn suppresses *NbMYB42*. Further, we examined whether auxin repressed *NbARFs* through transcriptional inhibition. Importantly, using promoter-GUS reporters, we found that auxin did not reduce *NbARF18La/b* mRNA levels through transcriptional

411 repression **(Fig. 6O)**. Therefore, it appears that auxin suppresses *NbARF* mRNA
412 levels through a post-transcriptional regulatory mechanism.
413
414 **Auxin-inducible miRNA *Nb*miR160c targets *NbARF* mRNA**
415 We explored the mechanisms by which auxin suppresses the transcript levels of
416 *NbARF18La* and *NbARF18Lb* via post-transcriptional regulation. Previous studies
417 have shown that plant miRNAs can negatively regulate the transcripts of *ARF* genes
418 (*46, 47*), and that auxin treatment can enhance miRNA accumulation in plants (*48*).
419 Therefore, we hypothesized that auxin-inducible, age-related miRNAs may be
420 responsible for the post-transcriptional regulation of these *ARF* genes. To test this
421 hypothesis, we analyzed miRNA sequencing data from 21-day-old *N. benthamiana*
422 plants and, through target prediction analysis, identified a miRNA, *Nb*miR160c,
423 which potentially targets the transcripts of *NbARF18La* and *NbARF18Lb*. Target site
424 analysis revealed that *Nb*miR160c specifically binds to the coding regions of
425 *NbARF18La* (1572 bp to 1590 bp) and *NbARF18Lb* (2099 bp to 2107 bp) **(Fig. 7A,**
426 **B)**. To validate this interaction, we artificially overexpressed *Nb*miR160c in 35-day-
427 old plants. This overexpression significantly reduced the mRNA levels of
428 *NbARF18La* and *NbARF18Lb* **(Fig. 7C; Fig. S9, A and B)**, suggesting direct
429 regulation of these transcripts by *Nb*miR160c.
430
431 Next, to pinpoint the exact cleavage sites of *NbARF18La* and *NbARF18Lb* by
432 *Nb*miR160c in juvenile plants, we conducted degradome sequencing on samples from
433 21-day-old plants. The analysis confirmed that *Nb*miR160c cleaves *NbARF18La* and
434 *NbARF18Lb* transcripts at the predicted target sites, as shown by the accumulation of
435 cleavage products at these regions **(Fig. 7, D and E)**. The red dots in **Fig. 7, D and E**
436 highlight the cleavage sites, aligning with the *Nb*miR160c target predictions.
437
438 To further confirm the regulatory role of *Nb*miR160c, we cloned the target sites of
439 *NbARF18La* and *NbARF18Lb* and fused them with a GFP tag. When these constructs
440 were transiently expressed in *N. benthamiana* leaves, co-expression with *Nb*miR160c
441 resulted in the suppression of GFP fluorescence **(Fig. 7, F and G; Fig. S9, C and D)**.
442 However, when the *Nb*miR160c target sites were mutated, GFP expression was
443 unaffected, even in the presence of *Nb*miR160c **(Fig. 7, F and G; Fig. S9, C and D)**.
444 Additionally, in co-expression assays with GUS-tagged target sites, *Nb*miR160c
445 suppressed the expression of wild-type GUS-tagged *NbARF18La* and *NbARF18Lb*
446 target sites, while the mutant target sites were unaffected **(Fig. 7H)**. We observed
447 similar results using LUC-tagged reporter constructs, where *Nb*miR160c suppressed
448 the activity of LUC reporter fused to the wild-type target sites of *NbARF18La* and
449 *NbARF18Lb*, but not the mutant constructs **(Fig. 7I)**. Collectively, these results
450 confirm that *Nb*miR160c directly targets the coding regions of *NbARF18La* and
451 *NbARF18Lb*, leading to their post-transcription repression. This auxin-inducable

452 miRNA thereby plays a crucial role in modulating *ARF* expression in *N. benthamiana*,
453 particularly during the juvenile stage.
454
455 ***Nb*miR160c regulates the expression of *NbMYB42* and *NbPAL6***
456 To explore the role of *Nb*miR160c in regulating the NbARF-NbMYB42 module-
457 mediated SA defense against whiteflies, we first overexpressed *Nb*miR160c in 35-
458 day-old plants. The overexpression resulted in a significant reduction in the mRNA
459 levels of *NbMYB42* and *NbPAL6* **(Fig. 8A)**, as well as in SA content and downstream
460 *NbPR1* expression **(Fig. 8B and Fig. S9E)**. Notably, the *Nb*miR160c-expressing 35-
461 day-old plants exhibited reduced defense against whiteflies **(Fig. 8C)**, indicating that
462 *Nb*miR160c negatively regulates plant anti-insect defense.
463
464 To validate the role of *Nb*miR160c in repressing *NbARF18La*/*b* and downstream SA
465 regulatory pathways in juvenile plants, we overexpressed an artificial target mimic of
466 *Nb*miR160c (mimic160c) in 21-day-old plants to inhibit its function **(Fig. S9F)**. As
467 expected, *NbARF18La* and *NbARF18Lb* transcript levels were significantly
468 upregulated in the treated plants **(Fig. 8D)**. Moreover, the *NbMYB42* and *NbPAL6*
469 mRNA levels **(Fig. 8E)**, SA levels **(Fig. S9G),** and *NbPR1* expression were also
470 significantly elevated in the mimic160c-overexpressing plants **(Fig. S9H)**.
471 Correspondingly, bioassays showed that whiteflies performed poorly on the
472 mimic160c-overexpressing plants, indicating enhanced defense **(Fig. 8F)**.
473
474 We then examined the effect of *Nb*miR160c on *NbARF*-promoted *NbMYB42*
475 transcription in plants at juvenile and adult stages. In 35-day-old plants,
476 overexpression of *Nb*miR160c repressed the activity of the *NbMYB42*pro-*LUC*
477 reporter **(Fig. S10A)**, whereas overexpression of mimic160c enhanced *NbMYB42*pro-
478 *LUC* reporter expression in 21-day-old plants **(Fig. S10B)**. When *Nb*miR160c was co-
479 expressed with *NbARF18La*, *NbARF18Lb*, or both, *NbMYB42pro* reporter expression
480 was significantly inhibited in 35-day-old plants **(Fig. 8G)**. These results demonstrate
481 that *Nb*miR160c represses *NbARF*-activated *NbMYB42* transcription. Similarly, we
482 confirmed that *Nb*miR160c is involved in repressing *NbPAL6* transcription in a
483 similar manner **(Fig. S10 C to E)**. Collectively, these findings show that *Nb*miR160c
484 negatively regulates *NbARF18La* and *NbARF18Lb*, thereby affecting the transcription
485 of *NbMYB42* and its downstream target *NbPAL6*.
486
487 **Auxin promotes the *Nb*miR160c level by enhancing its expression**
488 Next, we investigated the relationship between the *Nb*miR160c expression, plant age,
489 and phytohormones. We observed that *Nb*miR160c levels were significantly higher in
490 21-day-old plants compared to 35-day-old plants **(Fig. 8H)**. Given that auxin content
491 is typically higher in juvenile plants, we speculated that auxin might promote
492 *Nb*miR160c expression. To test this hypothesis, we treated 35-day-old plants, which
493 had naturally lower *Nb*miR160c levels, with IAA. The treatment significantly

increased *Nb*miR160c levels **(Fig. 8I)**. Additionally, we cloned the promoter of the *Nb*miR160c precursor from the *N. benthamiana* genome and fused it to GUS and LUC reporters. Upon IAA treatment, we observed enhanced reporter expression **(Fig. 8, J and K)**, confirming that auxin activates *Nb*miR160c transcription. These results indicate that auxin promotes *Nb*miR160c expression, thereby repressing the NbARF-NbMYB42-NbPAL6 module, which mediates whitefly defense in juvenile *N. benthamiana* plants.

Excessive SA impacts early plant growth by antagonizing auxin

We further examined the physiological implications of auxin-mediated suppression of SA in juvenile plants. To assess the impact of excessive SA on early plant growth, we treated 21-day-old plants with exogenous SA. These treated plants showed stunted growth **(Fig. 9A)** and, by the time they reached 35 days of age, had significantly reduced weight and height compared to untreated plants **(Fig. 9, B and C)**. These results, along with our earlier findings, suggest that while excessive SA enhances whitefly defense in juvenile plants, it also negatively impacts plant early growth.

Since auxin and SA pathways are known to antagonize each other, we examined whether SA inhibited early growth by interfering with the auxin pathway. Our results show that SA treatment significantly reduced the expression of the auxin synthesis genes *NbTAR2* and *NbYUC8* **(Fig. 9D)**, lowered auxin levels **(Fig. 9E)**, and decreased downstream *NbIAA29* expression **(Fig. 9F)** in juvenile plants. Conversely, the NahG plants, which have reduced SA levels, showed enhanced expression of auxin synthesis genes compared to wild-type plants at 35 days **(Fig. 9G)**. These results demonstrate that excessive SA in the early stages of plant development inhibits auxin accumulation, thereby hindering normal growth.

Discussion

In nature, plants exhibit enhanced defense against herbivorous insects as they age, with juvenile plants experiencing more frequent attacks than their adult counterparts. This observation has led to the development of the concepts of ARR and PVH; however, the precise mechanisms underlying these phenomena remain largely unknown. In this study, we elucidate the fine regulation of SA-mediated ARR against phloem-feeding whiteflies in plants **(Fig. 1)**. We highlight the importance of the PAL synthesis pathway in age-related intrinsic SA accumulation, identifying the key synthetic gene *NbPAL6* in *N. benthamiana* **(Fig. 2)**. Additionally, we identify the age-related upstream TF NbMYB42 and NbARF18La/b that are involved in SA regulation **(Fig. 3, and 4)**.

Furthermore, we provide insights into why SA-mediated resistance is not fully established in juvenile plants. Specifically, high levels of auxin in juvenile plants activate *Nb*miR160c, which silences the *NbARF18La/b* genes, ultimately impairing SA accumulation. This mechanism also prevents excessive SA from disrupting early plant growth. Our findings deepen the understanding of the PVH, demonstrating that juvenile plants exhibit lower herbivore tolerance while prioritizing urgent growth needs **(Fig. 10)**.

Our previous research has established the significant role of inducible SA in tobacco defense against whiteflies (*49*). In the current study, we found that the increased intrinsic SA levels associated with age also correlate with enhanced defense against whiteflies in adult plants **(Fig. 1)**. Although JA is crucial for plant defense against whiteflies (*49*), our findings indicate that the intrinsic JA levels did not vary with age across several Solanaceae species **(Fig. 1F)**, indicating that JA may not be a key phytohormonal signal in plant ARR against whiteflies. Recently, the role of SA in plant defense against phloem-feeding insects has gained attention (*50–52*), and our findings broaden the understanding of SA-mediated defenses from a novel perspective.

Moreover, we found the PAL pathway, rather than the ICS pathway, in SA biosynthesis changes at the transcriptional level with age in *N. benthamiana* **(Fig. 2B and C)**. Previous studies have shown the key role of *PAL* genes in SA accumulation in tobacco and other plant species (*38, 53, 54*). Here, we systematically analyzed *PAL* genes in *N. benthamiana* **(Fig. S2)** and determined the age-related upregulation of *NbPAL6* expression **(Fig. 2C)** and its role in age-related SA accumulation **(Fig. 2E)**. It is worth noting that our conclusion does not imply that *NbPAL6* is the sole *NbPAL* gene responsible for SA synthesis in *N. benthamiana*, as other *PALs* may contribute redundantly to SA synthesis. We suspect that additional *NbPAL*s may participate in SA

accumulation under various conditions, including biotic or abiotic stresses, warranting further investigation.

While extensive attention has been given to the upstream regulation of SA synthesis pathways, most studies have focused on the ICS pathway (*55*). The PAL pathway is known to contribute to the synthesis of numerous metabolic compounds in plants, such as flavonoids and lignin (*56*), but the regulation of *PAL* gene expression related to SA synthesis has been underexplored. For instance, in rice, the brown planthopper induces OsMYB30, which activates *OsPAL* gene expression, leading to increased SA and lignin accumulation and enhanced resistance (*38*). In our study, we demonstrated that the TF NbMYB42 activates *NbPAL6* expression by binding to its promoter, thereby enhancing SA levels and whitefly defense in an age-related constitutive, but not inducible, manner **(Fig. 3)**. Interestingly, in our previously published work, NbMYB42 was also shown to regulate lignin synthesis pathways in *N. benthamiana*, contributing to enhanced whitefly resistance (*39*). These observations combined highlight the necessity of MYB-PAL modules in plant SA and lignin synthesis, as well as their defense against phloem-feeding insects. In summary, our findings elucidate the mechanisms of age-related SA synthesis and regulation in plants, providing a valuable reference for future studies on the significance of age-enhanced SA in plant physiology and its induction in plant-pathogen and plant-insect interactions.

It is well established that SA and auxin signaling pathways often interact antagonistically (*57*). Elevated auxin levels correlate with reduced *PR* gene expression (*58, 59*) and increased susceptibility to pathogens (*59–61*). In this study, we found that increased auxin levels can also impact plant defense against phloem-feeding insects by antagonizing SA levels **(Fig. 6, A to F)**. Previous studies have indicated that auxin signaling may affect SA biosynthesis, although the underlying mechanisms remain largely unknown (*57, 59*). Our study revealed that auxin inhibits the expression of the key synthesis gene *NbPAL* and its transcriptional regulators, NbMYB42 and NbARF18La/b, thereby reducing SA biosynthesis **(Fig. 6, G to O)**. In addition, repression of auxin signaling by SA has been demonstrated in studies on plant growth. For example, SA treatment decreased biomass in Arabidopsis, an effect that was abolished in the *auxin resistant 3* (*axr3*) mutant background, which harbors an auxin-negative regulator (*62*). Similarly, we found that increased SA levels influenced auxin accumulation and related gene expression **(Fig. 9, D to F)**, leading to reduced growth in *N. benthamiana* plants **(Fig. 9, A to C)**. Collectively, these findings deepen our understanding of the crosstalk between SA and auxin, particularly regarding upstream biosynthesis.

Studies have shown that ARFs activate MYB TFs involved in various essential physiological processes (*63–66*). Our study complementarily reports that the two ARFs, NbARF18La and NbARF18Lb, positively regulate SA biosynthesis by

promoting SA-related MYB TFs, thereby enhancing plant defense against herbivores **(Fig. 4 and Fig. 5)**. Notably, the two ARFs we identified can interact with one another **(Fig. S6)**. Our findings indicate that auxin inhibits SA accumulation, positioning NbARFs as central hubs in this interaction. While ARFs are known participants in the antagonism between auxin and other phytohormones, such as ABA and JA (*40, 67*), little is reported regarding their relationship with SA. Previous studies have shown that the auxin-induced ARF7 represses the expression of SA-downstream *PR* genes that regulate bacterial infections in tomato plants (*68*). In contrast, we found that in *N. benthamiana* auxin represses the transcriptional activators NbARF18La/b **(Fig. 6)**, thereby negatively affecting upstream SA signaling.

Additionally, this work reveals the mechanism by which auxin represses NbARFs through miR160c-mediated post-transcriptional regulation **(Fig. 7)**. Prior studies have demonstrated that several miRNAs target *ARF* transcripts to regulate growth and development. For example, in Arabidopsis, miR160 targets *ARF10/16/17* (*69*), while miR167 antagonizes *ARF6/8* (*47*). Our findings further illuminate the relatively unexplored role of miR160c in regulating ARFs, suggesting a mechanism by which it fine-tunes plant defense against phloem-feeding insects **(Fig. 7 and Fig. 8)**.

Age-related changes in sRNA levels have been shown to play an important role in plant growth and stress responses. In Arabidopsis, the decline in the levels of miR156/7 with age drives plant maturation (*70, 71*), while an increase in miR172 with plant age promotes the transition toward adulthood and flowering (*72*). Notably, age-related miRNA gradients are also implicated in plant immunity against pathogens. For example, miR172b levels are very low during the early stage of seedling development but increase over time, enhancing pathogen immunity by reducing the expression of *TARGET OF EAT1/2* (*TOE1/2*), repressors of the immune receptor FLAGELLIN-SENSING2 (FLS2) (*73*). In this study, we demonstrate the role of age-related sRNA changes in regulating insect resistance. Specifically, the decrease in miRNA160c levels with age alleviates inhibition of its target defense-related TFs, thereby promoting insect resistance **(Fig. 8)**.

The regulation of miRNA levels in plants is complex, and influenced by various factors including phytohormones, which can either increase or decrease miRNA levels (*18, 74*). We found that auxin increased miR160c levels by promoting its transcription **(Fig. 8, J and K)**. The connections between miRNAs and phytohormones are an emerging area of research, with multiple recent studies highlighting the role of miRNAs in regulating plant phytohormonal pathways (*74, 75, 76*). As a supplementary finding, we revealed that auxin-induced miRNA can target key regulators involved in the antagonism of SA synthesis **(Fig. 10)**. These findings broaden our understanding of the molecular and physiological mechanisms underlying phytohormone interactions. Our work demonstrates, for the first time, the

role of miRNA in mediating the crosstalk between developmental auxin and defensive SA, balancing plant growth and defense **(Fig. 10)**.

Developing new crop varieties with improved product traits and enhanced stress resilience is a primary goal of global crop breeding, however, this effort is often limited by the growth-defense (G-D) trade-off (*76*). Consequently, the G-D trade-off has garnered increasing attention. However, the G-D balance in plants is not immutable; it can be influenced by various factors, such as developmental stage and environmental conditions. In this study, we specifically focused on the mechanisms underlying the trade-off between growth and insect resistance across different plant ages **(Fig. 10)**. We conclude that the auxin-miR160c module represses the ARFs-MYB-PAL module, mediating insect defense while ensuring early growth during the juvenile stage. As plants mature, this repression is gradually alleviated, allowing for the establishment of SA-mediated resistance alongside continued plant growth. These findings are likely to inspire further strategies for regulating crop growth and stress resistance by fine-tuning phytohormone interactions, key TFs, metabolic pathways, and miRNA levels. Importantly, genetic optimization in breeding programs must fully consider the age dynamics of plant-insect interactions to overcome the G-D trade-offs and develop ideal crop varieties.

Materials and Methods

Insect and plant materials

The *Bemisia tabaci* MEAM1 whitefly (*mtCOI* GenBank accession: GQ332577) was used in this study. Whiteflies were reared on cotton plants (*Gossypium hirsutum* cv. Zhemian 1793). Whitefly adults within 7 days post-emergence were used for experiments. Green peach aphids (*Myzus persicae*) were reared on tobacco (*N. tabacum* cv. NC89), with adult winged aphids also taken at 7 days post-emergence for experiments. The western flower thrips (*Frankliniella occidentalis*) were similarly reared on cotton plants (*G. hirsutum* cv. Zhemian 1793). Adult thrips, within 7 days post-emergence, were taken in the experiments.

N. benthamiana seeds (accession LAB and line H2B-RFP), tobacco (*N. tabacum* cv. NC89), and tomato (*Solanum lycopersicum* cv. Hezuo903) were sown in a soil mixture composed of peat moss, perlite, and vermiculite in a ratio of 5:3:1 (v/v/v) and placed in climate chambers. After approximately 14 days, when the *N. benthamiana*, tobacco, and tomato seedlings had germinated in a seed starter tray, the resulting plants were transplanted into plastic pots for individual cultivation. *N. benthamiana* plants at 7 days post-transplanting (21 days old, 3–4 true leaves) were classified as juvenile plants (low resistance), while *N. benthamiana* plants at 21 days post-transplanting (35 days old, 8–9 true leaves) were referred to as adult plants (high resistance) **(Fig. 2D)**. For tobacco, 7 days post-transplanting (21 days old, 3–4 true leaves) were classified as juvenile plants and 21 days post-transplanting (35 days old, 6–7 true leaves) were classified as the adult plants. For tomatoes, 7 days post-transplanting (21 days old, 3–4 true leaves) were classified as juvenile plants and 21 days post-transplanting (35 days old, 8–9 true leaves) were classified as adult plants.

Insect-rearing plants and experimental plants were grown in climate chambers at Zhejiang University (Hangzhou, China) at 26 ± 1°C, 65 ± 10% relative humidity, and a photoperiod of 14 h light: 10 h dark. All the insect-plant interaction experiments were conducted under the same conditions.

Insect bioassay

Bioassays were conducted using the following methods and standards. The test plants were placed in specially designed nylon cages (30 cm × 30 cm × 30 cm, 120 mesh), and the test insects (5 female and 5 male adults of MEAM1 whitefly, 3 female adults of aphid, and 5 female and 5 male adults of thrip respectively) were released into each of the cages. After two days, the performance of insects (whitefly, survival rate, and fecundity; aphid, offspring number; thrips, survival rate) was observed and recorded.

For the age-related bioassays, 21-day-old and 35-day-old *N. benthamiana* plants were simultaneously prepared based on their growth timeline. Specifically, we first sowed

704 the initial batch of *N. benthamiana* and when these plants reached 14 days old, we
705 sowed the second batch. Both batches were grown in a strictly controlled environment
706 as described above. By the time the first batch reached 35 days, the second batch was
707 21 days old. These two batches of *N. benthamiana* were then used for subsequent
708 bioassays as mentioned above. Bioassays related to gene and miRNA functions were
709 performed through *Agrobacterium*-mediated transient gene expression or VIGS. Two
710 days after gene overexpressing or 14 days after gene silencing **(Fig. 2D)**, whiteflies
711 were released onto the plants, and whitefly survival and fecundity were determined
712 after two days. For bioassays involving the external application of chemicals to the
713 plants, whitefly assessments commenced two days after chemical treatment.
714
715 Transient expression assays
716 The full-length cDNAs of the selected genes (*NbPAL6*, *NbMYB42*, and *NbARF18L*s)
717 were amplified via PCR using gene-specific primer pairs **(Table S2)**. The full-length
718 CDS sequences were inserted into pCAMBIA1305 vectors using the NovoRec plus
719 one-step PCR cloning kit (Novoprotein, Suzhou, China) to generate gene expression
720 constructs (pCAMBIA1305-*NbPAL6*-GFP, pCAMBIA1305-*NbMYB42*-GFP,
721 pCAMBIA1305-*NbARF18La*-GFP, and pCAMBIA1305-*NbARF18Lb*-GFP). For
722 transient expression in *N. benthamiana*, *Agrobacterium tumefaciens* strain EHA105
723 containing the respective vector was cultured overnight in LB medium at 28 °C.
724 Bacterial cultures were harvested by centrifugation, resuspended in buffer (10 mM
725 MES, pH 5.7, 10 mM $MgCl_2$, and 200 μM acetosyringone) to an OD600 of 0.8, and
726 infiltrated into leaves of 21-day-old or 35-day-old *N. benthamiana* using a needleless
727 syringe **(Fig. 2D)**. The infiltrated plants were then maintained in the previously
728 described climate chambers. Two days later, the treated plants were used for follow-
729 up experiments including bioassays and sample collection **(Fig. 2D)**.
730
731 VIGS assays
732 A 300 bp fragment of the target gene from *N. benthamiana* was identified using the
733 VIGS tool on the Sol Genomics Network (https://vigs.solgenomics.net/). The gene
734 fragment was amplified from *N. benthamiana* cDNA via PCR and cloned into the
735 pTRV2 vector. The resulting plasmid was introduced into *A. tumefaciens* strain
736 EHA105 by electroporation. Following cultivation, bacterial cells were harvested,
737 resuspended, and adjusted to an OD600 of 0.2. The cultures were incubated at room
738 temperature for at least 3 h. For leaf infiltration, cultures containing pTRV1 were
739 mixed in equal volumes with those containing pTRV2:00 (empty vector, control),
740 pTRV2-*NbPAL6*, pTRV2-*NbMYB42* or pTRV2-*NbARF18L*s. These suspensions were
741 infiltrated into 21-day-old *N. benthamiana* leaves using a 1 mL needleless syringe
742 **(Fig. 2D)**. Following infiltration, the *N. benthamiana* plants were maintained in the
743 same climate chamber conditions. Fourteen days later, the treated plants were used for
744 follow-up experiments, including bioassays and sample collection **(Fig. 2D)**.
745

746 Subcellular localization
747 The pCAMBIA1305-*NbMYB42*-GFP, pCAMBIA1305-*NbARF18La*-GFP,
748 pCAMBIA1305-*NbARF18Lb*-GFP, and pCAMBIA1305-GFP (empty vector)
749 constructs were used for subcellular localization. These constructs were infiltrated
750 into the leaves of *N. benthamiana* line H2B-RFP via *A. tumefaciens* strain EHA105.
751 Two days post-infiltration, GFP fluorescence signals were visualized using confocal
752 microscopy (Zeiss LSM710, Oberkochen, Germany).
753
754 RNA extraction and RT-qPCR analysis
755 Total RNA was extracted using *AG RNAex Pro* reagent (Accurate Biology, Changsha,
756 China). For mRNA, single-stranded cDNA was synthesized using the Evo *M-MLV* RT
757 Kit with gDNA Clean for qPCR Ver.2 (Accurate Biology Changsha, China). For plant
758 miRNA cDNA synthesis, the miRNA 1st strand cDNA synthesis kit (Accurate
759 Biology, Changsha, China) was used. RT-qPCR was conducted on a Bio-Rad CFX96
760 real-time PCR system (Bio-Rad, California, USA) with specific primers **(Table S2)**.
761 Data were analyzed with Bio-Rad CFX Manager Software, employing the $2^{-\Delta\Delta C_T}$
762 method. The *N. benthamiana* housekeeping gene *NbACTIN* served as the internal
763 control for gene expression analysis, and the expression of the *NbU6* snRNA genes
764 was employed as the internal control for miRNA level analysis.
765
766 Measurement of phytohormone content
767 For the quantification of phytohormones (SA, JA, and IAA), *N. benthamiana* leaves
768 were promptly excised and ground into powder in liquid nitrogen. Leaf powder (0.15
769 g) was mixed with 1 mL of HPLC-grade ethyl acetate (Sinopharm, Shanghai, China)
770 containing 10 ng D4-SA (Quality Control Chemicals, Spokane, WA, USA), 10 ng D6-
771 JA (Quality Control Chemicals, Spokane, WA, USA), and 5 ng D5-IAA (OlhemIm,
772 Shanghai, China). The mixture was fully vortexed and centrifuged. The supernatant
773 was collected and dried using a vacuum concentrator (Eppendorf AG, Hamburg,
774 Germany) at 30°C. The residue was resuspended in 110 μL of methanol: H_2O (50:50,
775 v/v), and the resulting supernatant was analyzed via high-performance liquid
776 chromatography-tandem mass spectrometry (TripleTOF 5600+; AB Sciex, Redwood
777 City, CA, USA).
778
779 Degradome sequencing
780 The degradome sequencing analysis, performed according to established protocols
781 from a previous study (*77*), was outsourced to Lianchuan Biotechnology Co., Ltd.
782 Poly(A) RNA was purified from total plant RNA using poly-T oligo magnetic beads
783 (Invitrogen, Carlsbad, CA, USA) through two rounds of purification. First-strand
784 cDNA synthesis was performed with a 3′-adapter random primer, followed by size
785 selection using AMPureXP beads (Beckman Coulter, Indianapolis, IN, USA) and
786 PCR amplification. The final cDNA library had an average insert size of 200–400 bp.
787 Sequencing was carried out with 50 bp single-end reads on an Illumina HiSeq 2500

788 (Illumina, San Diego, CA, USA). CleaveLand 3.0 and TargetFinder 50 were
789 employed to identify potential sliced targets of known miRNAs.
790
791 Y1H and Y2H assay
792 For the Y1H assay, approximately 2 kb of the promoter regions of the target genes
793 (*NbPAL6* and *NbMYB42*) were inserted into the pAbAi vector to construct the bait
794 plasmids. These plasmids were integrated into the Y1HGold yeast strain via
795 polyethylene glycol-mediated transformation, following in the Yeast User Manual
796 PT4087-1 (Clontech, Shiga, Japan). The CDSs of the corresponding TFs NbMYB42
797 and NbARF18La/b were cloned into the pGADT7 vector. The relevant vectors were
798 co-expressed in Y1H yeast cells and screened with varying concentrations of
799 Aureobasidin A (AbA, TaKaRa, Beijing, China).
800
801 For the Y2H assays, the full-length CDSs of the target proteins NbARF18La and
802 NbARF18Lb were ligated into pGBKT7 and pGADT7 (Clontech, Shiga, Japan),
803 respectively. The paired vectors were transformed into Y2HGold yeast strain cells via
804 PEG/LiAc transformation and grown on SD −Leu/−Trp medium. After 3–4 days of
805 incubation, the clones were transferred onto SD −Leu/−Trp/−His/−Ade medium and
806 incubated at 29°C for 3–4 days. The primers used for vector construction related to
807 the Y1H and Y2H assays are listed in **Table S2**.
808
809 Histochemical GUS activity assays
810 For the reporter constructs, the promoters of the target genes *NbPAL6* and *NbMYB42*
811 were introduced into the pBI121 vector containing a *GUS* gene-coding region.
812 Simultaneously, the full-length cDNAs of the corresponding target TFs (NbMYB42
813 and NbARF18La/b) were inserted into the pCAMBIA1305 vector to generate effector
814 constructs (pCAMBIA1305-*NbMYB42*-GFP, pCAMBIA1305-*NbARF18La*-GFP,
815 pCAMBIA1305-*NbARF18Lb*-GFP, as described in the Transient expression assays
816 section). The pCAMBIA1305 vector without the target CDS was used as the negative
817 control (empty effector). These vectors were transformed into *A. tumefaciens* strain
818 EHA105, and reporter vectors were co-transformed with the corresponding effector or
819 control vectors for transient expression. GUS activity was assessed using a GUS
820 histochemical assay kit (Coolaber, Beijing, China) according to the manufacturer's
821 instructions. GUS expression was visualized through staining and documented using
822 an iPhone 13 Pro Max (Apple, California, USA).
823
824 Dual-luciferase assays
825 For the reporter construct, the promoters of the target genes (*NbPAL6* and *NbMYB42*)
826 were inserted into the reporter vector pGreenII 0800-LUC. Effector constructs,
827 including pCAMBIA1305-*NbMYB42*-GFP, pCAMBIA1305-*NbARF18La*-GFP,
828 pCAMBIA1305-*NbARF18Lb*-GFP, and the empty vector pCAMBIA1305, were the
829 same as those used in the Histochemical GUS activity assays. These vectors were

transformed into *A. tumefaciens* EHA105 (pSoup). In this system, LUC expression was driven by the target gene promoters, while REN was driven by the *CaMV 35S* promoter as an internal control. The reporter and corresponding effector constructs were transiently transformed into *N. benthamiana* leaves. After a three-day incubation, LUC signals were measured using the Dual-Luciferase Reporter Assay Kit (Vazyme, Nanjing, China) and analyzed on a FlexStation 3 Multi-Mode Microplate Reader (Molecular Devices, San Jose, CA, USA). Relative luciferase activity was calculated based on LUC: REN ratios.

ChIP assay

Leaves transformed with pCAMBIA1305-*NbMYB42*-GFP, pCAMBIA1305-*NbARF18La*-GFP, or pCAMBIA1305-*NbARF18Lb*-GFP (as described in the Transient expression assay), were collected for ChIP assays. The experiment followed established protocols using the same transient gene expression system (*78*). Briefly, transformed *N. benthamiana* leaves were harvested and fixed with 1% formaldehyde. The fixation was quenched by adding 1 × PBS buffer containing 0.125 M glycine under vacuum for 5 min. Chromatin DNA was sonicated to fragments of approximately 200–300 bp. The chromatin complexes were immunoprecipitated (IP) by Protein G Agarose (Beyotime, Shanghai, China) with an anti-GFP monoclonal antibody (Beyotime, Shanghai, China). The co-IP DNA was recovered at 65°C, purified, and analyzed by qPCR with SYBR qPCR Mix (Accurate Biology, Changsha, China) with gene-specific primers **(Table S2)**. The relative fold enrichment was calculated using leaves transformed with the pCAMBIA1305-GFP (empty vector) as a control.

EMSA assay

To prepare the test TF proteins for EMSA, the CDS of NbMYB42 was fused into the GST-tagged pGEX-6P-1 vector to generate NbMYB42-GST. The NbARF18La CDS was fused into the His-tagged pET28a-SUMO vector, generating NbARF18La-His-SUMO, and the NbARF18Lb CDS was fused into the MBP-tagged pMAL-c5x vector, generating NbARF18Lb-MBP. These fusion proteins were expressed in *E. coli* BL21 cells using 0.2 mM isopropyl-β-D-thiogalactopyranoside (IPTG) and purified. For protein purification, NbMYB42-GST was purified through GST-affinity chromatography (Beyotime, Shanghai, China), NbARF18Lb-MBP using MBPSep Dextrin Agarose Resin 6FF (Yeasen, Shanghai, China) and NbARF18La-His with Ni NTA Beads 6FF (Smart-Lifesciences, Changzhou, China).

Putative binding sites in the target gene promoters were predicted by Jasper (https://jaspar.elixir.no/). For the NbMYB42 and *NbPAL6* promoter interaction, biotin-labeled probes were designed based on the P3 sequence (GGTGGTTGTTGAGAGG) of the *NbPAL6* promoter **(Fig. 3G; Table S2)**, with a mutated version (AAAAAAAAAAAAAAAA) serving as the mutant probe. For the interaction

872 between NbARF18La/b and the *NbMYB42* promoter, biotin-labeled probes targeting
873 the AuxRE element P2 sequence (TGTCTC) were designed **(Fig. 4, G and H; Table**
874 **S2)**, with a mutated version (AAAAAA) as the control. Cold competitors (10-, 20-,
875 and 50-fold excess) of unlabeled probes were included in the reactions. Probes were
876 labeled using the EMSA Probe Biotin Labeling Kit (Beyotime, Shanghai, China).
877 Approximately 300 ng of the fusion protein was incubated with 30 ng of labeled
878 probes, and specific binding was assessed via the Chemiluminescent EMSA Kit
879 (Beyotime, Shanghai, China) following the manufacturer's instructions.
880 Chemiluminescent imaging was performed with the ChemiDoc Touch system (Bio-
881 Rad, California, USA). Labeled probes incubated with GST, His-SUMO, and MBP
882 proteins served as negative controls.
883
884 Pull-down assay
885 Pull-down assays were conducted to determine the interaction of NbARF18La and
886 NbARF18Lb. The recombinant proteins NbARF18La-His and NbARF18Lb-MBP
887 obtained in the above-mentioned EMSA assay were further used in this test. For MBP
888 pull-down, MBPSep Dextrin Agarose Resin (Yeasen, Shanghai, China) is prepared by
889 washing them with PBS and then incubating them with MBP-bait protein
890 NbARF18Lb or control MBP protein. After washing, the beads are incubated with
891 His-tagged interacting protein NbARF18La at 4°C for 3 h. Then the MBP beads
892 underwent four washes with washing buffer (20 mM phosphate buffer, 500 mM NaCl,
893 100 mM imidazole, pH 7.4) and were then collected using collecting buffer (20 mM
894 phosphate buffer, 500 mM NaCl, 500 mM imidazole, pH 7.4). The eluted samples
895 were separated by SDS-PAGE and detected by an anti-MBP (Affinity Bioscience,
896 Jiangsu, China) antibody and an anti-His antibody (Proteintech, Wuhan, China).
897
898 Bimolecular fluorescence complementation (BiFC) assay
899 The CDSs of *NbARF18La* and *NbARF18Lb* were inserted into p2YN and p2YC
900 vectors, respectively. *A. tumefaciens* EHA105 cells carrying p2YN constructs were
901 combined with cells containing p2YC constructs at a 1:1 ratio. This mixture was then
902 infiltrated into the leaves of the *N. benthamiana* H2B-RFP line. After three days of
903 incubation, fluorescence was visualized under a laser confocal microscope (Zeiss
904 LSM710, Oberkochen, Germany).
905
906 Exogenous application of phytohormones
907 The target compound was dissolved in methanol (for SA, IAA, and NAA) or dimethyl
908 sulfoxide (DMSO) (for Yucasin and L-Kyn) to produce the stock solution. Lanolin
909 was selected as a slow-release medium. The lanolin was heated to a liquid state and
910 the stock solution was added to the lanolin to create the final mixture: SA at 1 mM;
911 IAA and NAA at 1, 25, and 50 μM; Yucasin and L-Kyn at 50 μM. All the compounds
912 were purchased from Aladdin, Shanghai, China. The lanolin solution containing the
913 target compounds was transferred to a 1 mL sterile syringe and stored at -20°C.

914
915 Exogenous SA was applied to 21-day-old and 35-day-old *N. benthamiana* plants. IAA
916 and NAA were applied to 35-day-old plants, while Yucasin and L-Kyn were applied to
917 21-day-old plants. For application, 0.25 mL of lanolin was squeezed from the syringe
918 and gently smeared along the midvein at the base of the leaves using latex-gloved
919 fingers. After two days **(Fig. 2D)**, the treated plants were used in bioassays or for
920 sample collection for further experiments.
921
922 Transient expression and functional inhibition of miRNA in *N. benthamiana*
923 To overexpress target miRNA *Nb*mi160c in *N. benthamiana*, the precursor sequences
924 of *Nb*miR160c were synthesized by GenScript (Nanjing, China) and inserted into the
925 pCAMBIA1300 vector through specific primers **(Table S2; Fig. S9A)**. The constructs
926 were infiltrated into 35-day-old *N. benthamiana* plants, and after two days **(Fig. 2D)**,
927 the treated plants were used in bioassays or for sample collection for further
928 experiments.
929
930 To inhibit the *Nb*miR160c function, a target mimicry (mimic160c) expression system
931 was introduced. The precursor sequences of mimic160c were synthesized by
932 GenScript (Nanjing, China) and inserted into the pCAMBIA1300 vector using
933 specific primers **(Table S2; Fig. S9A and F)**. The constructs were infiltrated into 21-
934 day-old *N. benthamiana* plants, and after two days **(Fig. 2D)**, the treated plants were
935 used for bioassays or sample collection for further experiments.
936
937 MiRNA targeting validation
938 GFP, GUS, and LUC reporter systems were used to investigate the cleavage of
939 *NbARF18La* and *NbARF18Lb* targets by *Nb*miR160c. For the GFP reporter, the
940 *Nb*miR160c target site of *NbARF18La* and *NbARF18Lb* mRNA, as well as its mutant
941 form **(Fig. S9C)** were cloned into the pCAMBIA1305-GFP vector to construct GFP
942 sensors through specific primers **(Table S2; Fig. S9D)**. The constructs of the target
943 site and mutant target site were co-infiltrated with pCAMBIA1300-*Nb*miR160c
944 through *A. tumefaciens* strain EHA105. After two days of infiltration, GFP
945 fluorescence was observed using confocal microscopy, as described above. For the
946 GUS and LUC reporters, the *Nb*miR160c target site of *Nb*ARF18La and *Nb*ARF18Lb
947 mRNA, along with its mutant form, were cloned into the pCAMBIA121-GUS and
948 pGreenII 0800-LUC vectors, respectively, to construct GUS and LUC sensor through
949 specific primers **(Table S2; Fig. S9D)**. These constructs were co-infiltrated with
950 pCAMBIA 1300-*Nb*miR160c. After two days of infiltration, GUS and LUC activity
951 was examined using the previously described method.
952
953 MiRNA dual-luciferase assay
954 Co-expression of the LUC reporter and *Nb*miR160c was carried out to evaluate the
955 influence of *Nb*miR160c on downstream genes. The effectors pCAMBIA1300-pre-

*Nb*miR160c, pCAMBIA1300-premimic160c, and pCAMBIA1300 (empty vector control) were co-expressed with LUC reporters linked to the *NbMYB42* or *NbPAL6* promoters. After two days of infiltration, LUC activity was examined using the method mentioned method. The combination of effectors and reporters is shown in **Fig. 10 A to D**.

The system was also used to evaluate the possible influence of *Nb*miR160c on NbPAL6 transcription when NbARFs were overexpressed. The *LUC* gene linked to the *NbPAL6* promoter or *NbMYB42* promoter was used as the reporter respectively. pCAMBIA1305-NbARFs plus pCAMBIA1300-pre-*Nb*miR160c, and pCAMBIA1305-NbARFs plus pCAMBIA1300 (empty vector control) were co-infiltrated with the reporter into the leaves of *N. benthamiana*. LUC activity for the different combinations was detected and compared. The combinations of effectors and reporters are shown in **Fig. 8G** and **Fig. S10 E**.

Statistical analysis

All data were analyzed using IBM SPSS Statistics 22.0 and visualized using GraphPad Prism 9. Statistical significance was determined using Student's *t*-test (two-tailed) or one-way ANOVA, followed by Fisher's least significant difference (LSD) test.

Reference

1. D. Walters, M. Heil, Costs and trade-offs associated with induced resistance. *Physiol. Mol. Plant Pathol.* **71**, 3–17 (2007).
2. D. Cipollini, C. B. Purrington, J. Bergelson, Costs of induced responses in plants. *Basic Appl. Ecol.* **4**, 79–89 (2003).
3. M. Erb, P. Reymond, Molecular interactions between plants and insect herbivores. *Annu. Rev. Plant Biol.* **70**, 527–557 (2019).
4. G. A. Howe, G. Jander, Plant immunity to insect herbivores. *Annu. Rev. Plant Biol.* **59**, 41–66 (2008).
5. J. A. Gatehouse, Plant resistance towards insect herbivores: a dynamic interaction. *New Phytol.* **156**, 145–169 (2002).
6. A. R. Zangerl, C. E. Rutledge, The probability of attack and patterns of constitutive and induced defense: a test of optimal defense theory. *Am. Nat.* **147**, 599–608 (1996).
7. P. W. Price, The plant vigor hypothesis and herbivore attack. *Oikos* **62**, 244–251 (1991).
8. S. W. Makhabu, C. Skarpe, H. Hytteborn, Z. D. Mpofu, The plant vigour hypothesis revisited – how is browsing by ungulates and elephant related to woody species growth rate? *Plant Ecol.* **184**, 163–172 (2006).
9. T. Rankenberg, B. Geldhof, H. Van Veen, K. Holsteens, B. Van De Poel, R. Sasidharan, Age-dependent abiotic stress resilience in plants. *Trends Plant Sci.* **26**, 692–705 (2021).
10. M. Develey-Rivière, E. Galiana, Resistance to pathogens and host developmental stage: a multifaceted relationship within the plant kingdom. *New Phytol.* **175**, 405–416 (2007).
11. L. Hu, L. Yang, Time to fight: molecular mechanisms of age-related resistance. *Phytopathology* **109**, 1500–1508 (2019).
12. J. H. Kim, H. R. Woo, J. Kim, P. O. Lim, I. C. Lee, S. H. Choi, D. Hwang, H. G. Nam, Trifurcate feed-forward regulation of age-dependent cell death involving *miR164* in *Arabidopsis*. *Science* **323**, 1053–1057 (2009).
13. Y.-B. Mao, Y.-Q. Liu, D.-Y. Chen, F.-Y. Chen, X. Fang, G.-J. Hong, L.-J. Wang, J.-W. Wang, X.-Y. Chen, Jasmonate response decay and defense metabolite accumulation contributes to age-regulated dynamics of plant insect resistance. *Nat. Commun.* **8**, 13925 (2017).
14. Z. He, S. Webster, S. Y. He, Growth–defense trade-offs in plants. *Curr. Biol.* **32**, R634–R639 (2022).
15. M. Vanstraelen, E. Benková, Hormonal interactions in the regulation of plant development. *Annu. Rev. Cell Dev. Biol.* **28**, 463–487 (2012).
16. A. Robert-Seilaniantz, M. Grant, J. D. G. Jones, Hormone crosstalk in plant disease and defense: more than just jasmonate-salicylate antagonism. *Annu. Rev. Phytopathol.* **49**, 317–343 (2011).

17. M. L. Berens, H. M. Berry, A. Mine, C. T. Argueso, K. Tsuda, Evolution of hormone signaling networks in plant defense. *Annu. Rev. Phytopathol.* **55**, 401–425 (2017).
18. X. Song, Y. Li, X. Cao, Y. Qi, MicroRNAs and their regulatory roles in plant–environment interactions. *Annu. Rev. Plant Biol.* **70**, 489–525 (2019).
19. J. Curaba, M. B. Singh, P. L. Bhalla, miRNAs in the crosstalk between phytohormone signalling pathways. *J. Exp. Bot.* **65**, 1425–1438 (2014).
20. M. Altmann, S. Altmann, P. A. Rodriguez, B. Weller, L. Elorduy Vergara, J. Palme, N. Marín-de La Rosa, M. Sauer, M. Wenig, J. A. Villaécija-Aguilar, J. Sales, C.-W. Lin, R. Pandiarajan, V. Young, A. Strobel, L. Gross, S. Carbonnel, K. G. Kugler, A. Garcia-Molina, G. W. Bassel, C. Falter, K. F. X. Mayer, C. Gutjahr, A. C. Vlot, E. Grill, P. Falter-Braun, Extensive signal integration by the phytohormone protein network. *Nature* **583**, 271–276 (2020).
21. S.-S. Liu, P. J. De Barro, J. Xu, J.-B. Luan, L.-S. Zang, Y.-M. Ruan, F.-H. Wan, Asymmetric mating interactions drive widespread invasion and displacement in a whitefly. *Science* **318**, 1769–1772 (2007).
22. S. Liu, J. Colvin, P. J. De Barro, Species concepts as applied to the whitefly *Bemisia tabaci* systematics: how many species are there? *J. Integr. Agric.* **11**, 176–186 (2012).
23. P. J. De Barro, S.-S. Liu, L. M. Boykin, A. B. Dinsdale, *Bemisia tabaci*: a statement of species status. *Annu. Rev. Entomol.* **56**, 1–19 (2011).
24. S. Kanakala, M. Ghanim, Global genetic diversity and geographical distribution of *Bemisia tabaci* and its bacterial endosymbionts. *PLoS One* **14**, e0213946 (2019).
25. X.-W. Wang, P. Li, S.-S. Liu, Whitefly interactions with plants. *Curr. Opin. Insect Sci*. (2017).
26. M. Inbar, D. Gerling, Plant-mediated interactions between whiteflies, herbivores, and natural enemies. *Annu. Rev. Entomol.* **53**, 431–448 (2008).
27. X.-W. Wang, S. Blanc, Insect transmission of plant single-stranded DNA viruses. *Annu. Rev. Entomol.* **66**, 389–405 (2021).
28. S. Morin, P. W. Atkinson, L. L. Walling, Whitefly–plant interactions: an integrated molecular perspective. *Annu. Rev. Entomol.* **69**, 503–525 (2024).
29. J. Bally, H. Jung, C. Mortimer, F. Naim, J. G. Philips, R. Hellens, A. Bombarely, M. M. Goodin, P. M. Waterhouse, The rise and rise of *Nicotiana benthamiana* : a plant for all reasons. *Annu. Rev. Phytopathol.* **56**, 405–426 (2018).
30. M. M. Goodin, D. Zaitlin, R. A. Naidu, S. A. Lommel, *Nicotiana benthamiana*: its history and future as a model for plant–pathogen interactions. Mol. Plant-Microbe Interact. **2015 (1)**, 28–39 (2015).
31. W. Han, J. Wang, F. Zhang, S. Ji, Y. Zhong, Y. Liu, S. Liu, X. Wang, A new feature of the laboratory model plant *Nicotiana benthamiana* : dead-end trap for sustainable field pest control. *Plants People Planet*, ppp3.10484 (2024).

1057 32. X. Wang, H. Han, R. Xie, B. Zhang, W. Ge, X. Ji, S. Liu, W. Wang,
1058 Metabolic and molecular insights into *Nicotiana benthamiana* trichome exudates: an
1059 ammunition depot for plant resistance against insect pests. *Plant, Cell Environ.* (2024)
1060 doi: 10.1111/pce.15135.
1061 33. X.-Y. Zhang, W.-H. Han, F.-B. Zhang, J.-X. Wang, S.-S. Liu, X.-W. Wang,
1062 Attraction of *Nicotiana benthamiana* to *Bemisia tabaci* is related to a chemical signal
1063 in plant volatile, undecane. *Pest Manage. Sci.* (2024) doi: 10.1002/ps.8411.
1064 34. T. Gaffney, L. Friedrich, B. Vernooij, D. Negrotto, G. Nye, S. Uknes, E.
1065 Ward, H. Kessmann, J. Ryals, Requirement of salicylic acid for the induction of
1066 systemic acquired resistance. *Science* **261**, 754–756 (1993).
1067 35. Y. Peng, J. Yang, X. Li, Y. Zhang, Salicylic acid: biosynthesis and signaling.
1068 *Annu. Rev. Plant Biol.* **72**, 761–791 (2021).
1069 36. C. J. Arntzen, Using tobacco to treat cancer. *Science* **321**, 1052–1053 (2008).
1070 37. B. Craven-Bartle, B. Pascual, F. M. Ca, A Myb transcription factor regulates
1071 genes of the phenylalanine pathway in maritime pine. *Plant J.* (2013).
1072 38. J. He, Y. Liu, D. Yuan, M. Duan, Y. Liu, Z. Shen, C. Yang, Z. Qiu, D. Liu, P.
1073 Wen, J. Huang, D. Fan, S. Xiao, Y. Xin, X. Chen, L. Jiang, H. Wang, L. Yuan, J. Wan,
1074 An R2R3 MYB transcription factor confers brown planthopper resistance by
1075 regulating the phenylalanine ammonia-lyase pathway in rice. *Proc. Natl. Acad. Sci.*
1076 *U.S.A.* **117**, 271–277 (2020).
1077 39. F.-B. Zhang, S.-X. Ji, J.-G. Yang, X.-W. Wang, W.-H. Han, Genome-wide
1078 analysis of MYB family in *Nicotiana benthamiana* and the functional role of the key
1079 members in resistance to *Bemisia tabaci*. *Int. J. Biol. Macromol.* **235**, 123759 (2023).
1080 40. C. Cancé, R. Martin-Arevalillo, K. Boubekeur, R. Dumas, Auxin response
1081 factors are keys to the many auxin doors. *New Phytol.* **235**, 402–419 (2022).
1082 41. D. R. Boer, A. Freire-Rios, W. A. M. van den Berg, T. Saaki, I. W. Manfield,
1083 S. Kepinski, I. López-Vidrieo, J. M. Franco-Zorrilla, S. C. de Vries, R. Solano, D.
1084 Weijers, M. Coll, Structural basis for DNA binding specificity by the auxin-dependent
1085 ARF transcription factors. *Cell* **156**, 577–589 (2014).
1086 42. T. J. Guilfoyle, The PB1 domain in auxin response factor and Aux/IAA
1087 proteins: a versatile protein interaction module in the auxin response. *Plant Cell* **27**,
1088 33–43 (2015).
1089 43. D. A. Korasick, Defining a two-pronged structural model for PB1
1090 (Phox/Bem1p) domain interaction in plant auxin responses. *J. Biol. Chem.* **290**,
1091 12868-78 (2015).
1092 44. S.-B. Li, Z.-Z. Xie, C.-G. Hu, J.-Z. Zhang, A review of auxin response
1093 factors (ARFs) in plants. *Front. Plant Sci.* **7** (2016).
1094 45. K. Jiang, T. Asami, Chemical regulators of plant hormones and their
1095 applications in basic research and agriculture. *Biosci. Biotechnol. Biochem.* **82**, 1265–
1096 1300 (2018).
1097 46. E. Marin, V. Jouannet, A. Herz, A. S. Lokerse, D. Weijers, H. Vaucheret, L.
1098 Nussaume, M. D. Crespi, A. Maizel, miR390, *Arabidopsis TAS3* tasiRNAs, and their

1099 *AUXIN RESPONSE FACTOR* targets define an autoregulatory network quantitatively
1100 regulating lateral root growth. *Plant Cell* **22**, 1104–1117 (2010).
1101 47. N. Liu, S. Wu, J. Van Houten, Y. Wang, B. Ding, Z. Fei, T. H. Clarke, J. W.
1102 Reed, E. Van Der Knaap, Down-regulation of *AUXIN RESPONSE FACTORS 6* and *8*
1103 by microRNA 167 leads to floral development defects and female sterility in tomato.
1104 *J. Exp. Bot.* **65**, 2507–2520 (2014).
1105 48. J.-J. Wang, H.-S. Guo, Cleavage of *INDOLE-3-ACETIC ACID*
1106 *INDUCIBLE28* mRNA by microRNA847 upregulates auxin signaling to modulate
1107 cell proliferation and lateral organ growth in Arabidopsis. *Plant Cell* **27**, 574–590
1108 (2015).
1109 49. Y.-X. Liu, W.-H. Han, J.-X. Wang, F.-B. Zhang, S.-X. Ji, Y.-W. Zhong, S.-S.
1110 Liu, X.-W. Wang, Differential induction of JA/SA determines plant defense against
1111 successive leaf-chewing and phloem-feeding insects. *J. Pest Sci.* (2024) doi:
1112 10.1007/s10340-024-01821-x.
1113 50. T. Züst, A. A. Agrawal, Mechanisms and evolution of plant resistance to
1114 aphids. *Nat. Plants* **2**, 15206 (2016).
1115 51. R. Blundell, J. E. Schmidt, A. Igwe, A. L. Cheung, R. L. Vannette, A. C. M.
1116 Gaudin, C. L. Casteel, Organic management promotes natural pest control through
1117 altered plant resistance to insects. *Nat. Plants* **6**, 483–491 (2020).
1118 52. D. Mertens, M. Fernández de Bobadilla, Q. Rusman, J. Bloem, J. C. Douma,
1119 E. H. Poelman, Plant defence to sequential attack is adapted to prevalent herbivores.
1120 *Nat. Plants* **7**, 1347–1353 (2021).
1121 53. M. B. Shine, J. Yang, M. El-Habbak, P. Nagyabhyru, D. Fu, D. Navarre, S.
1122 Ghabrial, P. Kachroo, A. Kachroo, Cooperative functioning between phenylalanine
1123 ammonia lyase and isochorismate synthase activities contributes to salicylic acid
1124 biosynthesis in soybean. *New Phytol.* **212**, 627–636 (2016).
1125 54. D. Ogawa, N. Nakajima, S. Seo, I. Mitsuhara, H. Kamada, Y. Ohashi, The
1126 phenylalanine pathway is the main route of salicylic acid biosynthesis in *Tobacco*
1127 *mosaic virus*-infected tobacco leaves. *Plant Biotechnol.* **23**, 395–398 (2006).
1128 55. P. Ding, Y. Ding, Stories of salicylic acid: a plant defense hormone. *Trends*
1129 *Plant Sci.* **25**, 549–565 (2020).
1130 56. N. Dong, H. Lin, Contribution of phenylpropanoid metabolism to plant
1131 development and plant–environment interactions. *J. Integr. Plant Biol*. **63**, 180–209
1132 (2021)
1133 57. A. Robert-Seilaniantz, M. Grant, J. D. G. Jones, Hormone crosstalk in plant
1134 disease and defense: more than just jasmonate-salicylate antagonism. *Annu. Rev.*
1135 *Phytopathol.* **49**, 317–343 (2011).
1136 58. J.-E. Park, J.-Y. Park, Y.-S. Kim, P. E. Staswick, J. Jeon, J. Yun, S.-Y. Kim, J.
1137 Kim, Y.-H. Lee, C.-M. Park, GH3-mediated auxin homeostasis links growth
1138 regulation with stress adaptation response in *Arabidopsis*. *J. Biol. Chem.* **282**, 10036–
1139 10046 (2007).

1140 59. A. Robert-Seilaniantz, D. MacLean, Y. Jikumaru, L. Hill, S. Yamaguchi, Y.
1141 Kamiya, J. D. G. Jones, The microRNA miR393 re-directs secondary metabolite
1142 biosynthesis away from camalexin and towards glucosinolates. *Plant J.* **67**, 218–231
1143 (2011).
1144 60. L. Navarro, R. Bari, P. Achard, P. Lisón, A. Nemri, N. P. Harberd, J. D. G.
1145 Jones, DELLAs control plant immune responses by modulating the balance of
1146 jasmonic acid and salicylic acid signaling. *Curr. Biol.* **18**, 650–655 (2008).
1147 61. S. A. McClerklin, S. G. Lee, C. P. Harper, R. Nwumeh, J. M. Jez, B. N.
1148 Kunkel, Indole-3-acetaldehyde dehydrogenase-dependent auxin synthesis contributes
1149 to virulence of *Pseudomonas syringae* strain DC3000. *PLoS Pathog.* **14**, e1006811
1150 (2018).
1151 62. J. V. Canet, A. Dobón, F. Ibáñez, L. Perales, P. Tornero, Resistance and
1152 biomass in Arabidopsis: a new model for salicylic acid perception. *Plant Biotechnol.*
1153 *J.* **8**, 126–141 (2010).
1154 63. R. Ghelli, P. Brunetti, N. Napoli, A. De Paolis, V. Cecchetti, T. Tsuge, G.
1155 Serino, M. Matsui, G. Mele, G. Rinaldi, G. A. Palumbo, F. Barozzi, P. Costantino, M.
1156 Cardarelli, A newly identified flower-specific splice variant of *AUXIN RESPONSE*
1157 *FACTOR8* regulates stamen elongation and endothecium lignification in Arabidopsis.
1158 *Plant Cell* **30**, 620–637 (2018).
1159 64. X.-F. Xu, B. Wang, Y.-F. Feng, J.-S. Xue, X.-X. Qian, S.-Q. Liu, J. Zhou, Y.-
1160 H. Yu, N.-Y. Yang, P. Xu, Z.-N. Yang, AUXIN RESPONSE FACTOR17 directly
1161 regulates *MYB108* for anther dehiscence. *Plant Physiol.* **181**, 645–655 (2019).
1162 65. G. Qu, D. Peng, Z. Yu, X. Chen, X. Cheng, Y. Yang, T. Ye, Q. Lv, W. Ji, X.
1163 Deng, B. Zhou, Advances in the role of auxin for transcriptional regulation of lignin
1164 biosynthesis. *Funct. Plant Biol.* **48**, 743–754 (2021).
1165 66. W. Jiang, Y. Xia, X. Su, Y. Pang, ARF2 positively regulates flavonols and
1166 proanthocyanidins biosynthesis in *Arabidopsis thaliana*. *Planta* **256**, 44 (2022).
1167 67. Y. Li, S. Han, Y. Qi, Advances in structure and function of auxin response
1168 factor in plants. *J. Integr. Plant Biol.* **65**, 617–632 (2023).
1169 68. X. Kong, C. Zhang, H. Zheng, M. Sun, F. Zhang, M. Zhang, F. Cui, D. Lv, L.
1170 Liu, S. Guo, Y. Zhang, X. Yuan, S. Zhao, H. Tian, Z. Ding, Antagonistic interaction
1171 between auxin and SA signaling pathways regulates bacterial infection through lateral
1172 root in *Arabidopsis*. *Cell Rep.* **32**, 108060 (2020).
1173 69. J.-W. Wang, L.-J. Wang, Y.-B. Mao, W.-J. Cai, H.-W. Xue, X.-Y. Chen,
1174 Control of root cap formation by microRNA-targeted auxin response factors in
1175 Arabidopsis. *Plant Cell* **17**, 2204–2216 (2005).
1176 70. J. Gao, K. Zhang, Y.-J. Cheng, S. Yu, G.-D. Shang, F.-X. Wang, L.-Y. Wu, Z.-
1177 G. Xu, Y.-X. Mai, X.-Y. Zhao, D. Zhai, H. Lian, J.-W. Wang, A robust mechanism for
1178 resetting juvenility during each generation in *Arabidopsis*. *Nat. Plants* **8**, 257–268
1179 (2022).
1180 71. S. Bergonzi, M. C. Albani, E. V. Loren Van Themaat, K. J. V. Nordström, R.
1181 Wang, K. Schneeberger, P. D. Moerland, G. Coupland, Mechanisms of age-dependent

response to winter temperature in perennial flowering of *Arabis alpina*. *Science* **340**, 1094–1097 (2013).

72. C.-M. Zhou, T.-Q. Zhang, X. Wang, S. Yu, H. Lian, H. Tang, Z.-Y. Feng, J. Zozomova-Lihová, J.-W. Wang, Molecular basis of age-dependent vernalization in *Cardamine flexuosa*. *Science* **340**, 1097–1100 (2013).

73. Y. Zou, S. Wang, Y. Zhou, J. Bai, G. Huang, X. Liu, Y. Zhang, D. Tang, D. Lu, Transcriptional regulation of the immune receptor FLS2 controls the ontogeny of plant innate immunity. *Plant Cell* **30**, 2779–2794 (2018).

74. T. Li, N. Gonzalez, D. Inzé, M. Dubois, Emerging connections between small RNAs and phytohormones. *Trends Plant Sci.* **25**, 912–929 (2020).

75. P. Singh, P. Dutta, D. Chakrabarty, miRNAs play critical roles in response to abiotic stress by modulating cross-talk of phytohormone signaling. *Plant Cell Rep.* **40**, 1617–1630 (2021).

76. E. Shen, T. Zhao, Q. Zhu, Are miRNAs applicable for balancing crop growth and defense trade-off? *New Phytol.* **243**, 1670–1680 (2024).

77. W.-H. Han, J.-X. Wang, F.-B. Zhang, Y.-X. Liu, H. Wu, X.-W. Wang, Small RNA and degradome sequencing reveal important microRNA function in *Nicotiana tabacum* response to *Bemisia tabaci*. *Genes* **13**, 361 (2022).

78. T. Zhu, X. Zhou, L. Zhang, H. Zhang, P. Zhang, X. You, P. E. Jameson, T. Ma, L. Guo, Ethylene-induced *NbMYB4L* is involved in resistance against tobacco mosaic virus in *Nicotiana benthamiana*. *Mol. Plant Pathol.* **23**, 16-31 (2021).

Acknowledgments：

We thank Rong Jin from the Agricultural Experiment Station, Zhejiang University, for greenhouse management. We also thank Xiao-Dan Wu from the Analysis Center of Agrobiology and Environmental Sciences, Zhejiang University, for technical support in the detection and analysis of phytohormones.

Funding:

Financial support for this study was provided by:
National Natural Science Foundation of China (31925033, 32161143008)
National Key Research and Development Program (2022YFC2601002)

Author contributions:

Conceptualization: W.H., F.Z., J.W., and X.W.
Methodology: F.Z., W.H., and X.F.
Investigation: F.Z., W.H., S.J., J.W., X.F., and K.L.
Visualization: W.H. and F.Z.
Supervision: S.L. and X.W.
Writing—original draft: W.H. and F.Z.
Writing—review & editing: W.H., F.Z., S.J., and X.W.

Competing interests:

The authors declare that they have no competing interests.

Data and materials availability:

All data needed to evaluate the conclusions in the paper are present in the paper and/or the Supplementary Materials.

1227 **Figures**

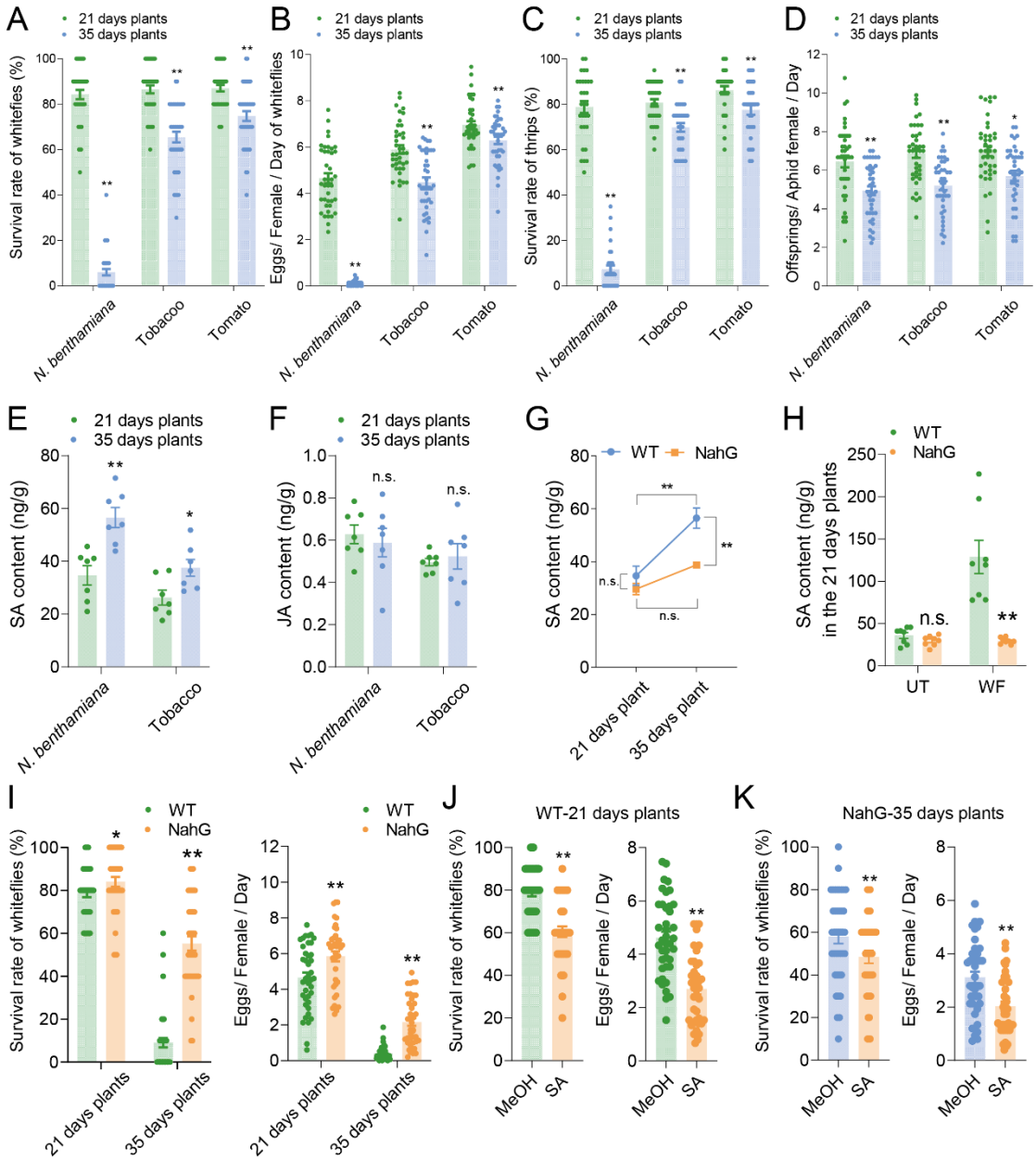

1228

1229 **Fig. 1. Plant age-related resistance against insects is regulated by SA.** (**A** and **B**)
1230 Survival rate and fecundity of whiteflies on 21-day-old and 35-day-old *N.*
1231 *benthamiana*, tobacco, and tomato plants. (**C**) Survival rate of thrips on 21-day-old
1232 and 35-day-old *N. benthamiana*, tobacco, and tomato plants. (**D**) Fecundity of aphids
1233 on *N. benthamiana*, tobacco, and tomato plants at 21-day and 35-day ages. (**E** and **F**)
1234 SA and JA levels in *N. benthamiana* and tobacco at different ages. (**G**) Temporal
1235 dynamics of SA content in wild-type and NahG *N. benthamiana* plants. (**H**) SA levels
1236 in 21-day-old wild-type and NahG *N. benthamiana* plants upon whitefly attack. (**I**)
1237 Survival rate and fecundity of whiteflies on 21-day-old and 35-day-old wild-type and
1238 NahG *N. benthamiana* plants. (**J**) Survival rate and fecundity of whiteflies on SA-
1239 treated (1 mM) 21-day-old wild-type *N. benthamiana* plants. (**K**) Survival rate and

fecundity of whiteflies on SA-treated (1 mM) 35-day-old NahG *N. benthamiana* plants. Values are means ± SE, $n = 40$ for **A**, **B**, **C**, **D**, **I**, **J**, and **K**, $n = 7$ for **E**, **F**, and **G**, $n = 8$ for **H**. Student's *t*-test (two-tailed) was used for significant difference analysis. n.s., not significant. *$P < 0.05$, **$P < 0.01$.

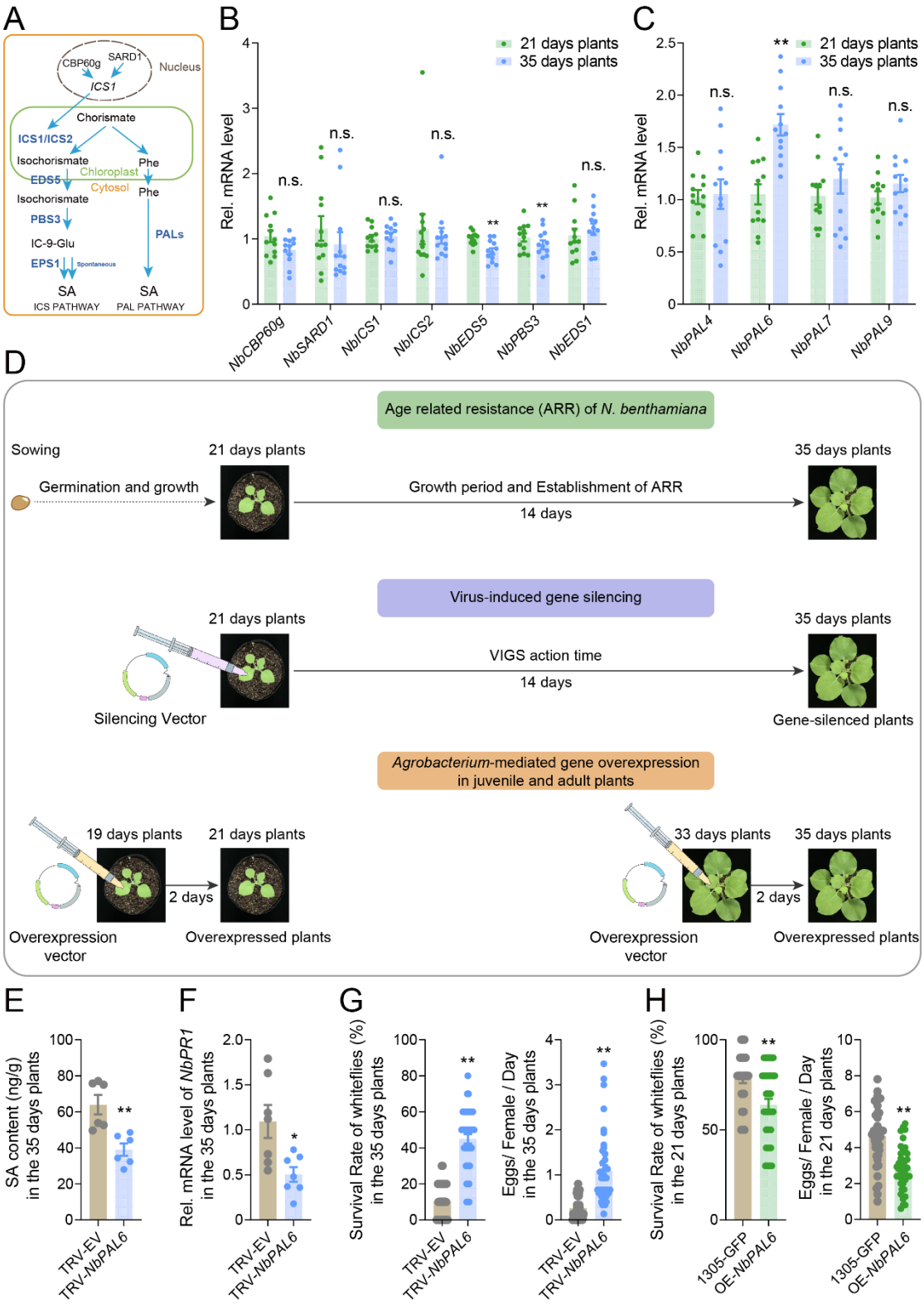

Fig. 2. ARR depends on the expression of the SA synthetic gene *NbPAL6*. (**A**) SA synthesis pathways in plants. (**B**) Expression levels of genes in the ICS pathways in 21-day-old and 35-day-old *N. benthamiana* plants. (**C**) Expression levels of *NbPAL* genes in 21-day-old and 35-day-old *N. benthamiana* plants. (**D**) Experimental design of VIGS and gene overexpression in *N. benthamiana* plants. In the VIGS system, the

pTRV2 vector is injected into 21-day-old plants, activating the silencing vector to inhibit target gene expression. Gene silencing typically became evident 14 days post-injection, aligning with the timeline for ARR establishment in *N. benthamiana*, making VIGS an effective tool for studying ARR-related gene functions. In comparison to control plants (receiving only the pTRV2 vector), 35-day-old plants subjected to gene silencing show reduced accumulation of target gene transcripts after reaching 21 days. Additionally, *Agrobacterium*-mediated gene overexpression enhances target gene mRNA levels in both 21-day-old and 35-day-old plants, allowing for gene function assessment across different developmental stages. For instance, when the pCAMBIA1305-GFP vector containing the target gene is introduced at 19 days, mRNA levels increase in the treated 21-day-old plants within two days. By comparing overexpressed plants to controls (those receiving the pCAMBIA1305-GFP vector without the target gene), the impact of target genes on resistance in 21-day-old plants can be assessed. This method was also used to evaluate the role of gene overexpression in enhancing resistance in 35-day-old plants. (**E**) SA levels in *NbPAL6*-silenced 35-day-old *N. benthamiana* plants. (**F**) Expression level of *NbPR1* in *NbPAL6*-silenced 35-day-old *N. benthamiana* plants. (**G**) Survival rate and fecundity of whiteflies on *NbPAL6*-silenced 35-day-old *N. benthamiana* plants. (**H**) Survival rate and fecundity of whiteflies on *NbPAL6*-overexpressed 21-day-old *N. benthamiana* plants. Values are mean ± SE, $n = 12$ for **B**, **C**, and **F**; $n = 6$ for **E**; $n = 40$ for **G** and **H**. Student's *t*-test (two-tailed) was used for significant difference analysis. n.s., not significant. $^{*}P < 0.05$, $^{**}P < 0.01$.

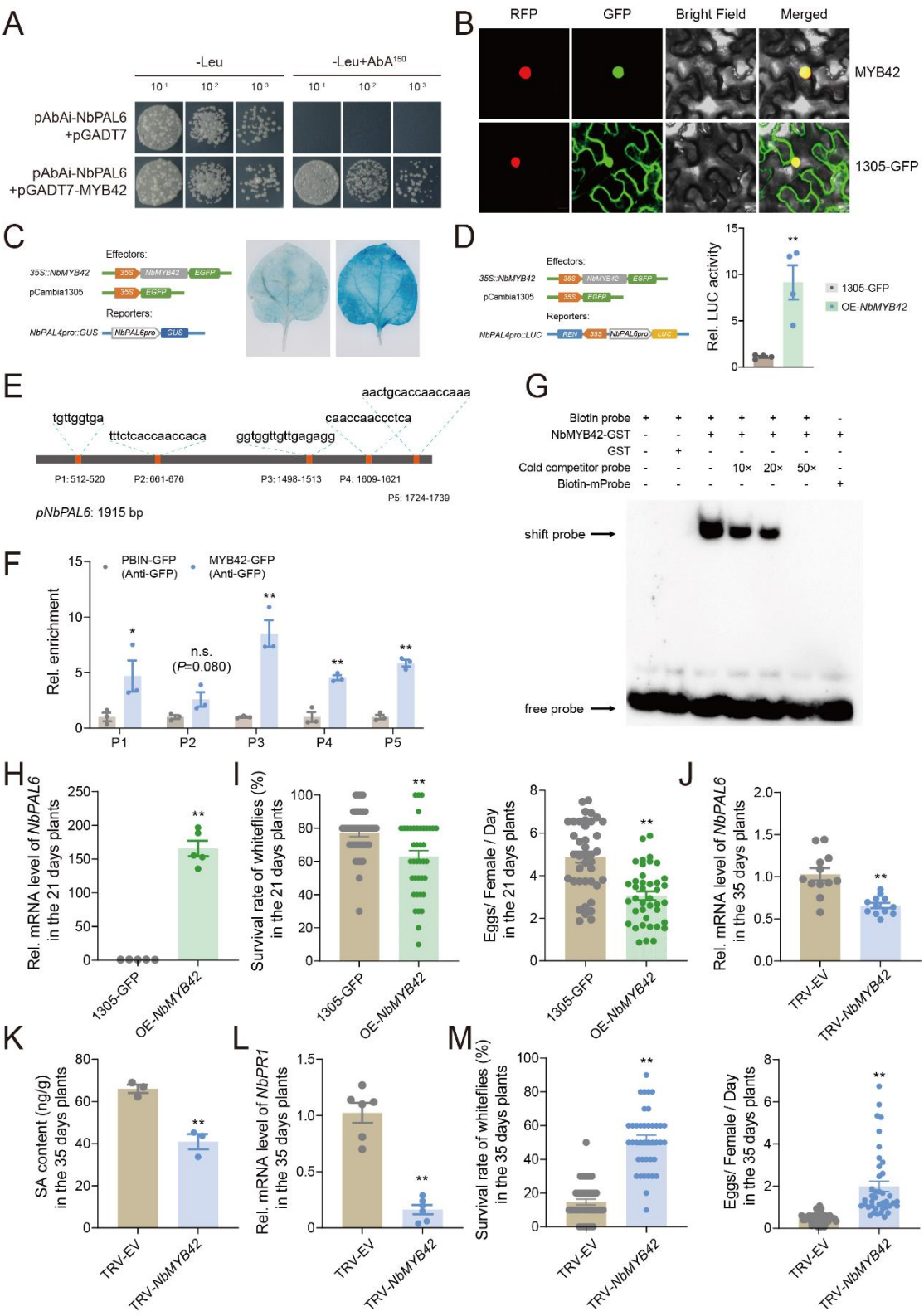

Fig. 3. NbMYB42 directly binds to the *NbPAL6* promoter to activate its transcription. (**A**) Yeast one-hybrid assay of the interaction between the *NbPAL6* promoter and NbMYB42. Gold yeast cells co-transformed with pAbAi-*NbPAL6pro* and pGADT7-*NbMYB42* plasmids were cultured on SD/-Leu medium with or without 150 ng ml^{-1}AbA for 3 days. The empty vector pGADT7 served as a negative control.

(**B**) Subcellular localization of NbMYB42 in *N. benthamiana*. NbMYB42-GFP (green fluorescent protein) was transiently expressed in *N. benthamiana* line H2B-RFP, with red fluorescent protein (RFP) as a nucleus marker and the empty *35S::GFP* vector used as a control. Scale bar: 20 μm. (**C**) Analysis of the interaction between the *NbPAL6* promoter and NbMYB42 in *N. benthamiana* leaves using a GUS staining assay. Diagrams on the left illustrate the reporter and effector vectors: *35S*, *CaMV 35S* promoter; *EGFP*, enhanced green fluorescent protein; *GUS*, β-glucuronidase. Representative photographs from several replicates are shown. (**D**) Analysis of the interaction between the *NbPAL6* promoter and NbMYB42 in *N. benthamiana* leaves using a dual-luciferase reporter assay. Diagrams on the left illustrate the reporter and effector vectors. *REN*, *Renilla luciferase*; *LUC*, *firefly luciferase*. The activity of REN was used as an internal control. (**E**) Schematic of the *NbPAL6* promoter, indicating possible binding sites P1 to P5 for the TF NbMYB42. (**F**) ChIP-qPCR assay of the enrichment of NbMYB42-GFP at the *NbPAL6* promoter with an anti-GFP antibody. PCR primer pairs were designed based on the position shown in (**E**). Element P3 (GGTGGTTGTTGAGAGG) is significantly enriched in NbMYB42-GFP plants. (**G**) EMSA results show NbMYB42-GST binding to the *NbPAL6* promoter *in vitro*. The NbMYB42-GST protein was incubated with a biotin-labeled probe to assess binding capacity. Labeled probes were incubated with and without GST protein as negative controls, and 10-, 20-, and 50-fold excess unlabeled probes were used as cold competitors. Biotin-mProbe was the labeled probe containing mutations in the P3 element of the *NbPAL6* promoter. (**H**) Expression level of *NbPAL6* in *NbMYB42*-overexpressed 21-day-old *N. benthamiana* plants. (**I**) Survival rate and fecundity of whiteflies on *NbMYB42*-overexpressed 21-day-old *N. benthamiana* plants. (**J**) Expression level of *NbPAL6* in *NbMYB42*-silenced 35-day-old *N. benthamiana* plant. (**K**) SA levels in *NbMYB42*-silenced 35-day-old *N. benthamiana* plants. (**L**) Expression level of SA downstream gene *NbPR1* in *NbMYB42*-silenced 35-day-old *N. benthamiana* plants. (**M**) Survival rate and fecundity of whiteflies on *NbMYB42*-silenced 35-day-old *N. benthamiana* plants. Values are mean ± SE, $n = 4$ for **D** and **F**; $n = 5$ for **H**; $n = 40$ for **I** and **M**; $n = 12$ for **J**; $n = 3$ for **K**; $n = 6$ for **L**. Student's *t*-test (two-tailed) was used for significant difference analysis. n.s., not significant. *$P < 0.05$, **$P < 0.01$.

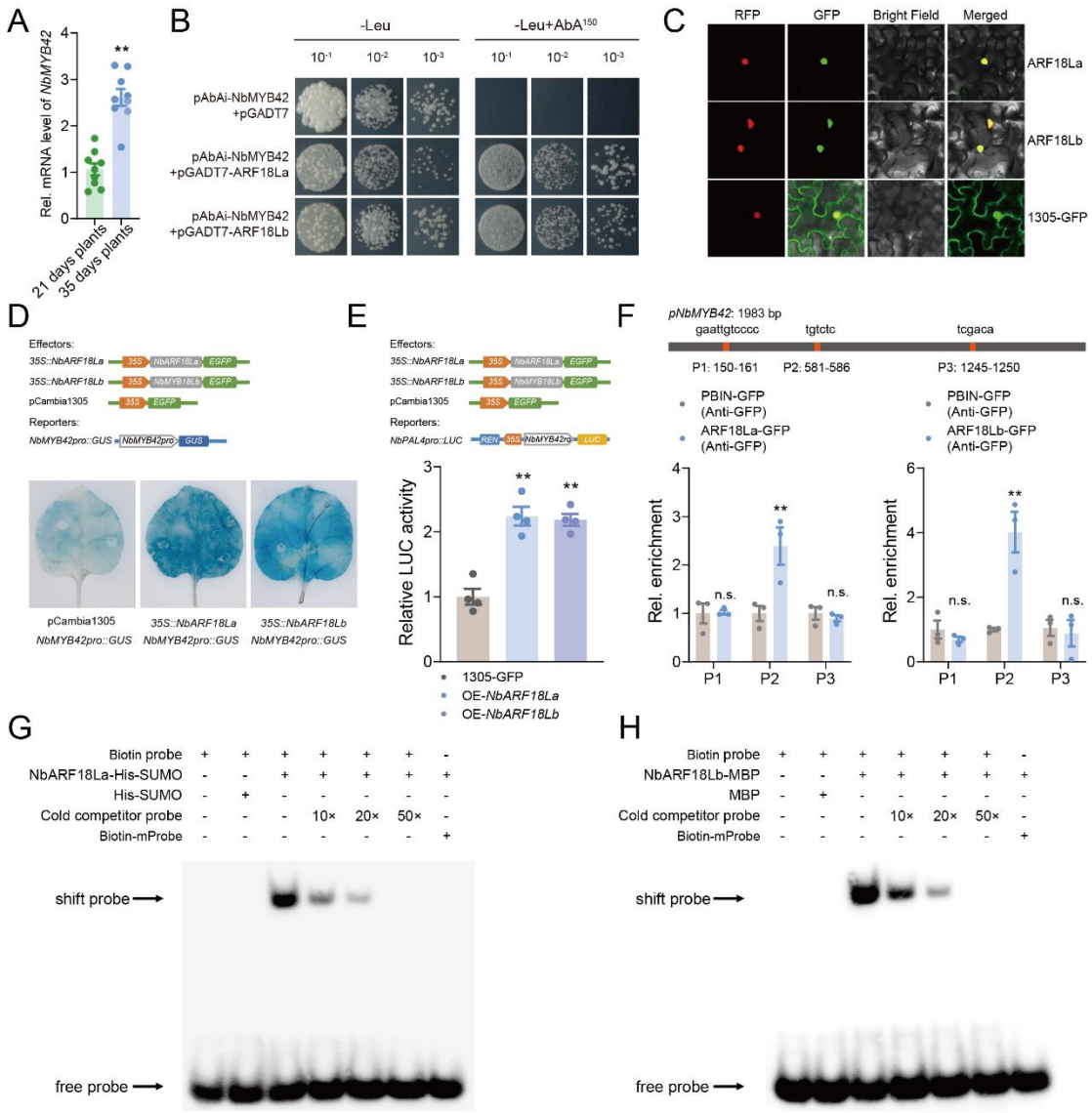

Fig. 4. NbARF18La and NbARF18Lb activate *NbMYB42* expression. (**A**) Expression levels of *NbMYB42* in 21-day-old and 35-day-old *N. benthamiana* plants. (**B**) Yeast one-hybrid assay of the interaction between the *NbMYB42* promoter and NbARF18La/b. Gold yeast cells co-transformed with pAbAi-*NbMYB42pro* and pGADT7-*NbARF18La/b* plasmids were cultured on SD/-Leu medium with or without 150 ng ml^{-1}AbA for 3 days. The empty vector pGADT7 was used as a negative control. (**C**) Subcellular localization of NbARF18La and NbARF18Lb in *N. benthamiana*. NbARF18La/b-GFP fusion proteins were transiently expressed in *N. benthamiana* line H2B-RFP. Red fluorescent protein (RFP) served as a nucleus marker, and the empty *35S*::*GFP* vector was used as a control. Scale bar: 20 µm. (**D**) GUS staining assay analyzing the interaction between the *NbMYB42* promoter and NbARF18La/b in *N. benthamiana* leaves. Diagrams on the top show the reporter and effector vectors. (**E**) Dual-luciferase reporter assay analyzing the interaction between the *NbMYB42* promoter and NbARF18La/b in *N. benthamiana* leaves. REN activity was used as an internal control. (**F**) Top: Schematic of the *NbMYB42* promoter

showing the distribution of possible NbARF binding sites. Bottom: ChIP-qPCR assay of the enrichment for NbARF18La/b-GFP protein at the *NbMYB42* promoter with an anti-GFP antibody. The PCR primer pair is based on the positions shown above. Element P2 (TGTCTC) is significantly enriched in NbARF18La/b-GFP plants. (**G** and **H**) EMSA showing binding of NbARF18La-His-SUMO and NbARF18Lb-MBP to the *NbMYB42* promoter *in vitro*. Proteins were incubated with a biotin-labeled fragment of the *NbMYB42* promoter (P2, TGTCTC). The labeled probe was incubated with and without His-SUMO or MBP protein as negative controls and 10-, 20- and 50-fold excess unlabeled probes were used as cold competitor probes. Biotin-mProbe refers to the labeled probe with mutations. Values are mean ± SE, $n = 9$ for **A**; $n = 4$ for **E**; $n = 3$ for **F**. Student's *t*-test (two-tailed) was used for significant difference analysis. n.s., not significant. $^{**}P < 0.01$.

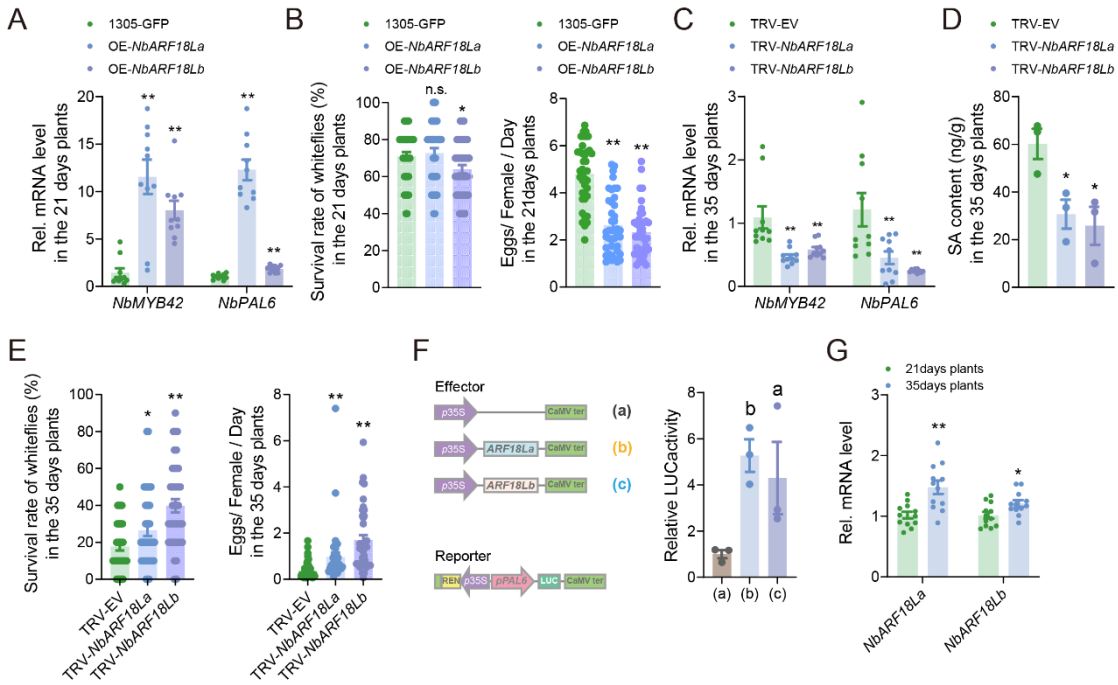

Fig. 5. NbARF18La and NbARF18Lb participate in whitefly defense. (**A**) Expression levels of *NbMYB42* and *NbPAL6* in *NbARF18La*/*18b*-overexpressed 21-day-old *N. benthamiana* plants. (**B**) Survival rate and fecundity of whiteflies on *NbMYB18a*/*b*-overexpressed 21-day-old *N. benthamiana* plants. (**C**) Expression levels of *NbMYB42* and *NbPAL6* in *NbARF18La*/*b*-silenced 35-day-old *N. benthamiana* plants. (**D**) SA levels in *NbMYB18La*/*b*-silenced 35-day-old *N. benthamiana* plants. (**E**)Survival rate and fecundity of whiteflies on the *NbMYB18La*/*b*-silenced 35-day-old *N. benthamiana* plants. (**F**) LUC activity was driven by the *NbPAL6* promoter when co-expressed with different effectors. (**G**) Expression levels of *NbARF18La/b* in 21-day-old and 35-day-old *N. benthamiana* plants. Values are mean ± SE, $n = 10$ for **A** and **C**; $n = 40$ for **B** and **E**; $n = 3$ for **D** and **F**; $n = 12$ for **G**. Student's *t*-test (two-tailed) was used for significant difference analysis. n.s., not significant. *$P < 0.05$, **$P < 0.01$.

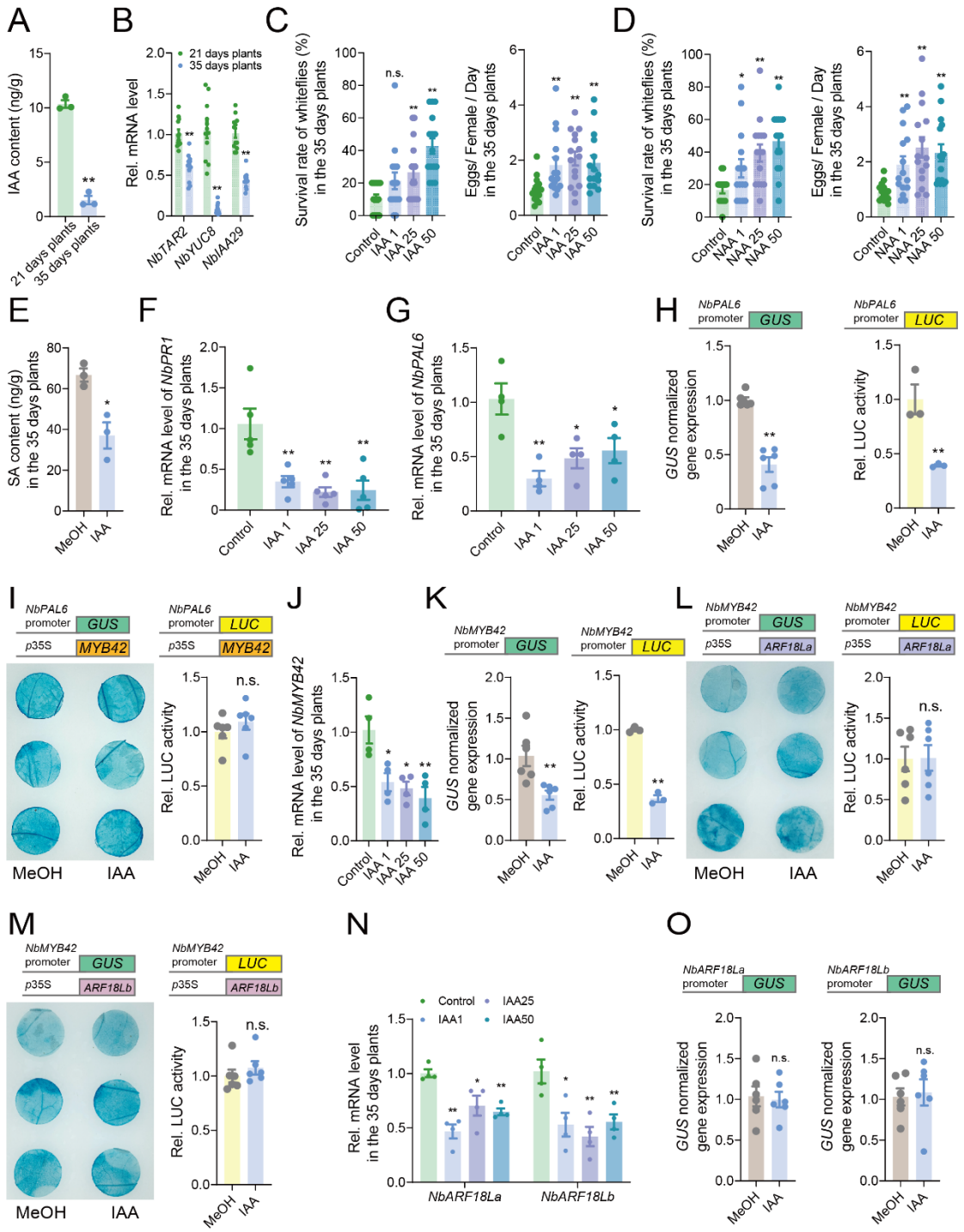

Fig. 6. Auxin suppresses NbARF18La/b-MYB42 mediated SA accumulation. (**A**) IAA levels in 21-day-old and 35-day-old *N. benthamiana* plants. (**B**) Expression level of *NbTAR2*, *NbYUC8*, and *NbIAA29* in 21-day-old and 35-day-old *N. benthamiana* plants. (**C**, **D**) Survival rate and fecundity of whiteflies on IAA/NAA-treated (1, 25, and 50 μM) 35-day-old *N. benthamiana* plants. (**E**) SA levels in IAA-treated (25 μM) 35-day-old *N. benthamiana* plants. (**F**) Expression level of *NbPR1* in IAA-treated (1, 25, and 50 μM) 35-day-old *N. benthamiana* plants. (**G**) Expression level of *NbPAL6* in IAA-treated (1, 25, and 50 μM) 35-day-old *N. benthamiana* plants. (**H**) Top: Schematic of the *GUS* reporter gene. Bottom: *GUS* reporter gene expression in mock-

and IAA-treated (25 μM) *pNbPAL6::GUS N. benthamiana* plants. (**I**) Top: Schematic of the *GUS* and *LUC* reporter genes and effector NbMYB42. Bottom: GUS / LUC activity co-expressed with *NbMYB42* in mock- or IAA-treated (25 μM) *pNbPAL6::GUS N. benthamiana* plants. (**J**) Expression level of *NbMYB42* in IAA-treated (1, 25, and 50 μM) 35-day-old *N. benthamiana* plants. (**K**) Top: Schematic of the *GUS* reporter genes. Bottom: *GUS* reporter gene expression in mock- and IAA-treated (25 μM) *pNbMYB42::GUS N. benthamiana* plants. (**L**) Top: Schematic of the *GUS* and *LUC* reporter gene and effector NbARF18La. Bottom, GUS / LUC activity co-expressed with *NbARF18La* in mock- and IAA-treated (25 μM) *pNbMYB42::GUS N. benthamiana* plants. (**M**) Top: Schematic of the *GUS* and *LUC* reporter gene and effector NbARF18Lb. Bottom: GUS / LUC activity co-expressed with *NbARF18Lb* in mock- and IAA-treated (25 μM) *pNbMYB42::GUS N. benthamiana* plants. (**N**) Expression level of *NbARF18La/b* in IAA-treated (1, 25, and 50 μM) 35-day-old *N. benthamiana* plants. (**O**) Top: Schematic of the *GUS* reporter gene. Bottom: *GUS* reporter gene expression in mock- and IAA-treated (25 μM) *pNbARF18La/b::GUS N. benthamiana* plants. Values are mean ± SE, $n = 3$ for **A** and **E**; $n = 12$ for **B**; $n = 15$ for **C** and **D**; $n = 5$ for **F**; $n = 4$ for **G**, **J** and **N**; $n = 6$ for **H**, **K**, and **O** (*GUS* normalized gene expression), $n = 3$ for **H** and **K** (Relative LUC activity); $n = 6$ for **I**, **L**, and **M** (Relative LUC activity). Student's *t*-test (two-tailed) was used for significant difference analysis. n.s., not significant. $^{*}P < 0.05$, $^{**}P < 0.01$.

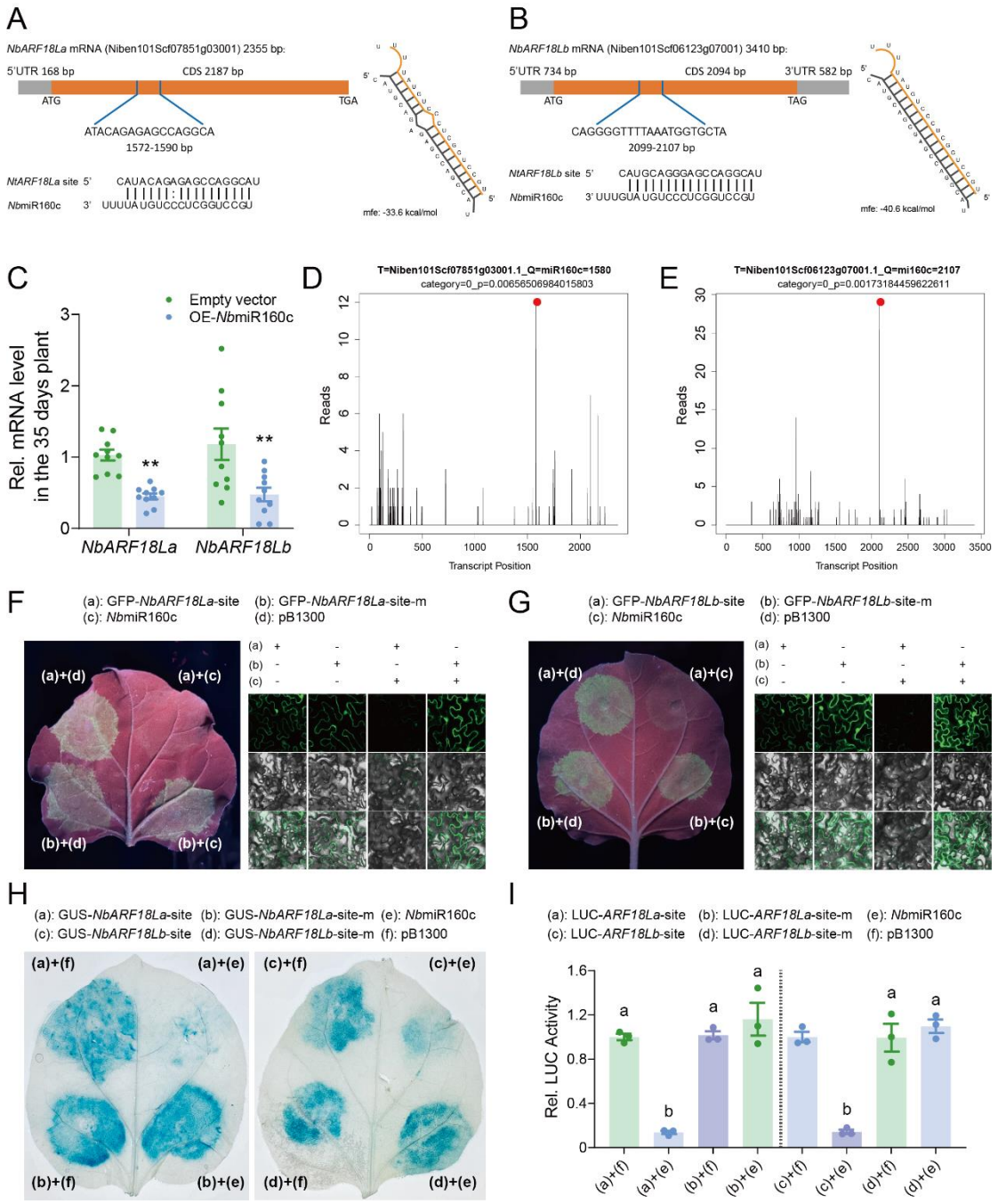

Fig. 7. Auxin-induced microRNA160c targets *NbARF18La/b* transcripts. (**A**) *Nb*miR160c targets *N. benthamiana NbARF18La* mRNA. CDS: Coding sequence; UTR: Untranslated regions; ATG: Initiation codon; TAA: Termination codon. (**B**) *Nb*miR160c targets *N. benthamiana NbARF18Lb* mRNA. (**C**) Expression of *NbARF18La/b* in *Nb*miR160c-expressing 35-day-old *N. benthamiana* plants. (**D**) Target plots (t-plots) of *Nb*miR160c and its target *NbARF18La* mRNA, validated via degradome sequencing. The red dot indicates the cleavage site of the *NbARF18La* transcript at 1572 bp, as analyzed by GSTAr (1.0) cleavage site prediction software. (**E**) Target plots (t-plots) of *Nb*miR160c and its target *NbARF18Lb* mRNA, showing cleavage at 2099 bp. (**F**, **G**) Camera (Left) and confocal (Right) images of GFP-*NbARF18La/b* target site and GFP-mutant site expression in *N. benthamiana* when

*Nb*miR160c was overexpressed. Top: GFP; Middle, Bright-field; Bottom: GFP/bright-field overlay. Scale bars, 40 μm. (**H**) GUS phenotype observed by histochemical staining showing GFP-*NbARF18La*/*b* target site and GFP-mutant site expression in *N. benthamiana* with overexpressed *Nb*miR160c. (**I**) LUC activity displaying LUC-*NbARF18Lb* target site and LUC-mutant site expression. Values are mean ± SE, n = 10 for **C**; n = 3 for **I**. Student's t-test (two-tailed) was used for significant difference analysis in **C**. $^{**}P < 0.01$. One-way ANOVA followed by Fisher's least significant difference (LSD) test was used for significant difference analysis in **I**. Bars with different lowercase letters indicate significant differences between treatments at $P < 0.05$.

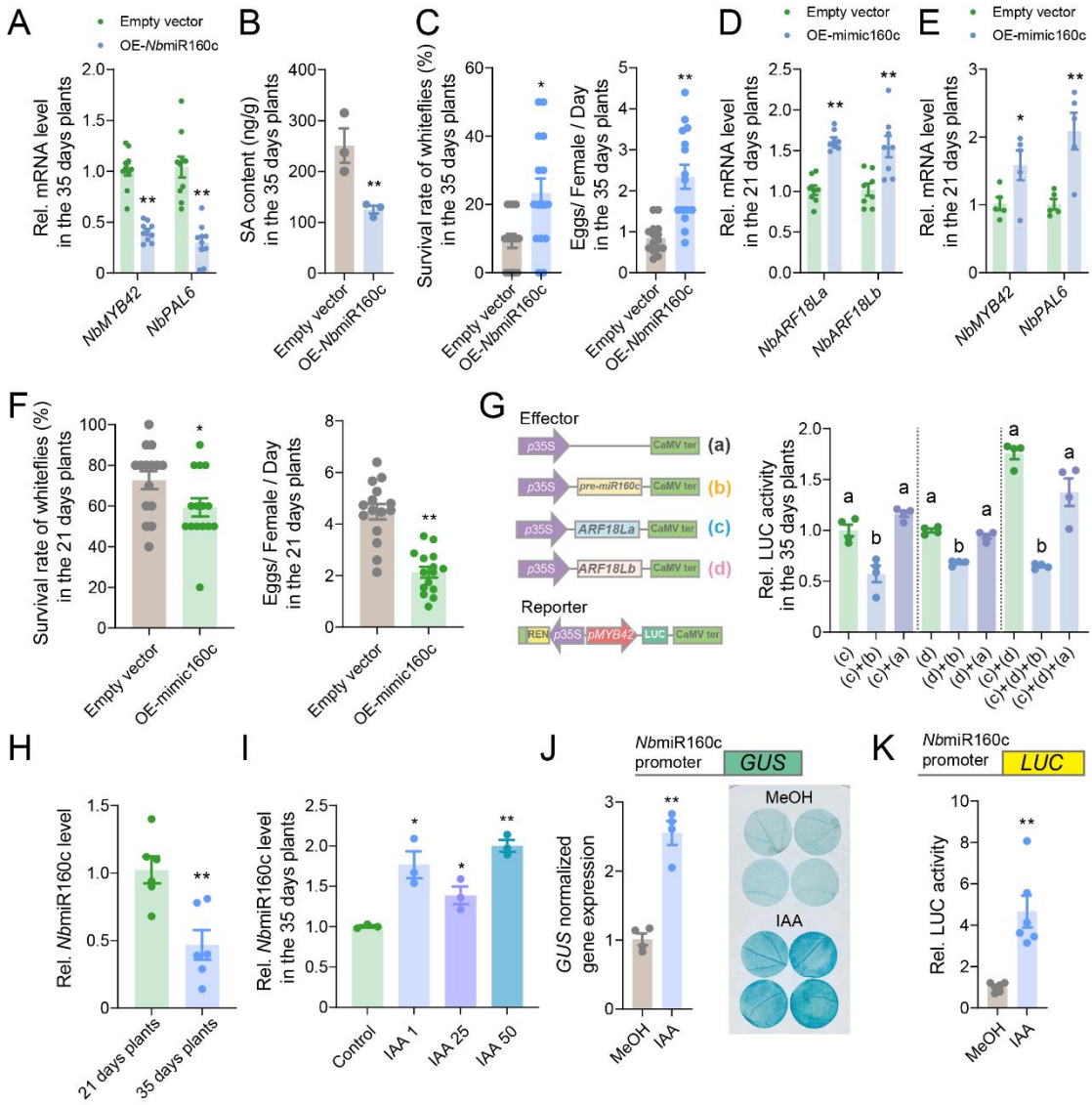

Fig. 8. Auxin-induced microRNA160c negatively regulates plant defense. (**A**) Expression of *NbMYB42* and *NbPAL6* in *Nb*miR160c-expressing 35-day-old *N. benthamiana* plants. (**B**) SA levels in *Nb*miR160c-expressing 35-day-old *N. benthamiana* plants. (**C**) Survival rate and fecundity of whiteflies on *Nb*miR160c-expressing 35-day-old *N. benthamiana* plants. (**D**) Expression of *NbARF18La/b* in mimic160c-expressing 21-day-old *N. benthamiana* plants. (**E**) Expression of *NbMYB42* and *NbPAL6* in mimic160c-expressing 21-day-old *N. benthamiana* plants. (**F**) Survival rate and fecundity of whiteflies on the mimic160c-expressed 21-day-old *N. benthamiana* plant. (**G**) Left: Schematic diagram showing effector and reporter vectors used in transient transcriptional activity assays in *N. benthamiana* leaves. Right: The LUC activity driven by the *NbMYB42* promoter when coexpressed with different effectors. (**H**) Expression level of *Nb*miR160c in 21-day-old and 35-day-old *N. benthamiana* plants. (**I**) *Nb*miR160c levels in IAA-treated (1, 25, and 50 μM) 35-day-old plants. (**J**) Top: Schematic of the *GUS* reporter gene; Bottom: *GUS* reporter gene expression and activity in mock- and IAA-treated (25 μM) *pNbmiR160c*::*GUS* *N. benthamiana* plants. (**K**) Top: Schematic of the *LUC* reporter gene; Bottom: *LUC*

1421 reporter gene expression and activity in mock- and IAA-treated (25 μM)
1422 *pNbmiR160c*::*LUC N. benthamiana* plants. Values are mean ± SE; $n = 10$ for **A**; $n = 3$
1423 for **B** and **I**; $n = 15$ for **C** and **F**; $n = 8$ for **D**; $n = 5$ for **E**; $n = 6$ for **H** and **K**; $n = 4$ for
1424 **G** and **J**. Student's *t*-test (two-tailed) was used for significant difference analysis in **A**,
1425 **B**, **C**, **D**, **E**, **F**, **H**, **I**, **J**, and **K**. *$P < 0.05$, **$P < 0.01$. One-way ANOVA followed by
1426 Fisher's least significant difference (LSD) test was used for significant difference
1427 analysis in **G**. Bars with different lowercase letters indicate significant differences
1428 between treatments at $P < 0.05$.

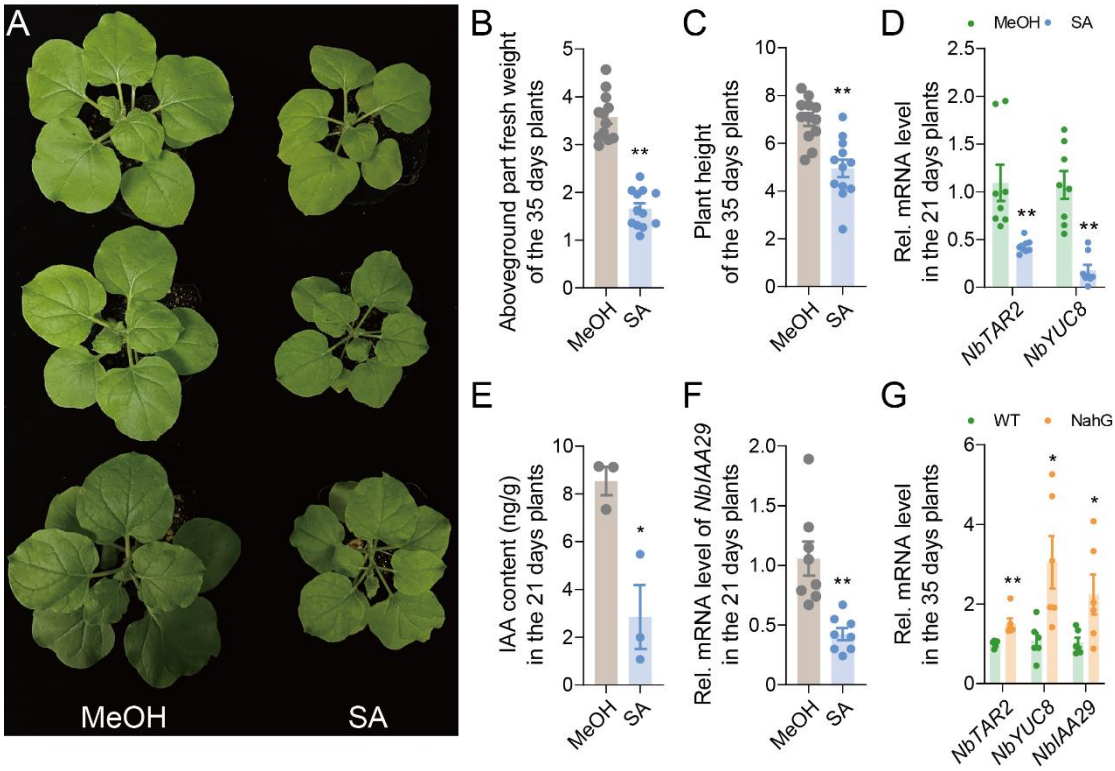

Fig. 9. Excessive SA impacts early plant growth by antagonizing auxin. (**A**) Photographs of 35-day-old *N. benthamiana* plants treated with SA starting at 21 days old. (**B**, **C**) Aboveground fresh weight **(B)** and plant height **(C)** of SA-treated (1 mM) *N. benthamiana* plants. (**D**) Expression levels of auxin synthesis genes *NbTAR2* and *NbYUC8* in 21-day-old *N. benthamiana* plants treated with 1 mM SA. (**E**) Auxin levels in 21-day-old *N. benthamiana* plants after successive SA treatment (1 mM). (**F**) Expression levels of auxin downstream gene *NbIAA29* in SA-treated (1 mM) 21-day-old *N. benthamiana* plants. (**G**) Expression of auxin pathway genes in 35-day-old wild type and NahG *N. benthamiana* plants. Values are mean ± SE, $n = 12$ for **B** and **C**; $n = 8$ for **D** and **F**; $n = 3$ for **E**; $n = 6$ for **G**. Student's *t*-test (two-tailed) was used for significant difference analysis. $^{*}P < 0.05$, $^{**}P < 0.01$.

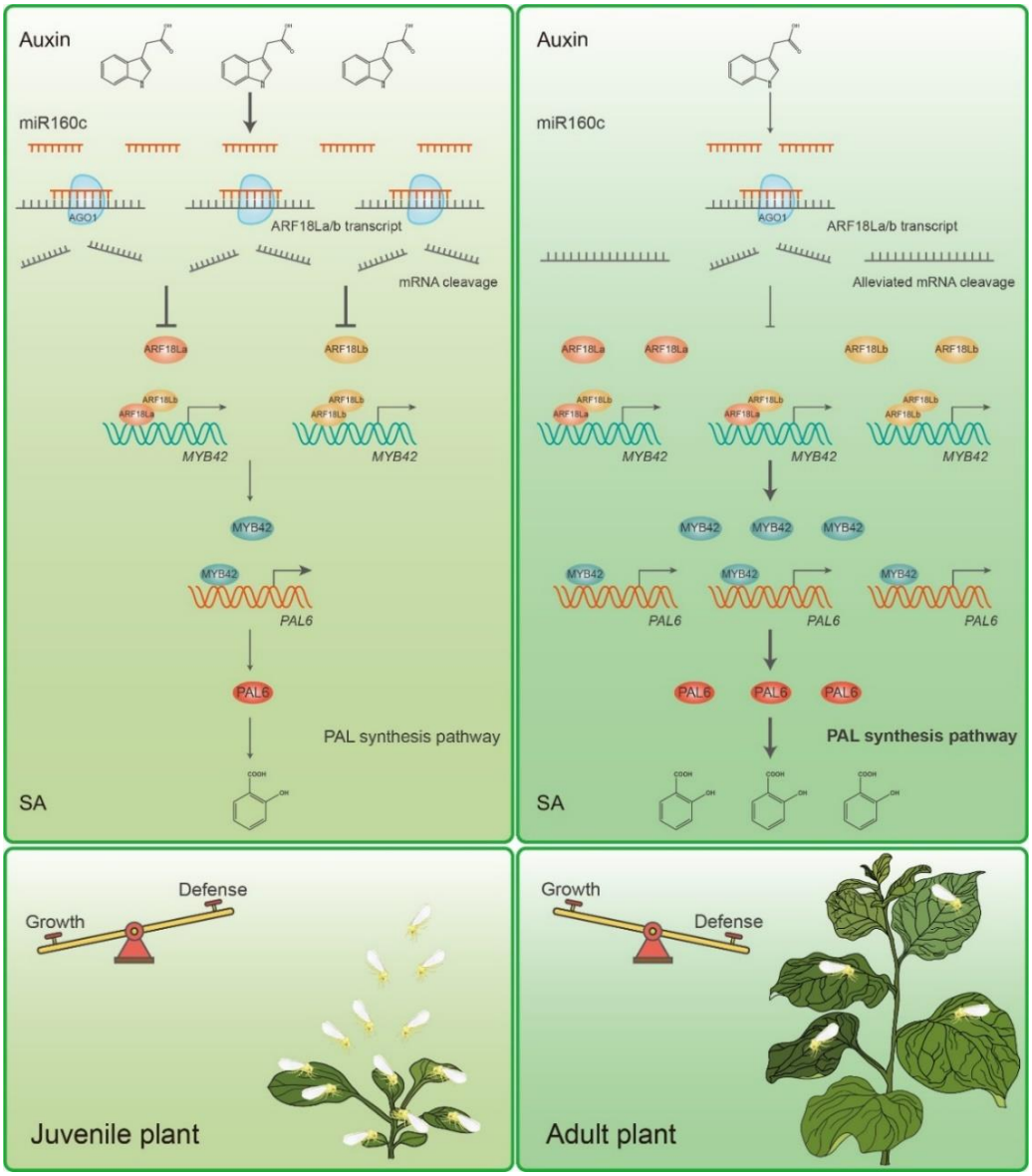

Fig. 10. Auxin-SA seesaw mediates the age-related balance between plant growth and herbivore defense. At juvenile stages, plants exhibit high auxin levels, promoting the expression of *Nb*miRNA160c. This miRNA targets *NbARF18La/b* transcripts, leading to their degradation via the plant ARGONAUTE1 (AGO1) protein. As a result, NbARF18La/b is degraded at an early age, inhibiting downstream expression of *NbMYB42* and *NbPAL6*. This repression of the NbARF18La/b-NbMYB42-NbPAL6 module limits anti-whitefly SA accumulation in juvenile plants. As plants mature, the auxin levels decrease, lifting the repression of NbARF18La/b. These two interacting ARF TFs directly bind to the promoter of the TF *NbMYB42*, activating its expression. NbMYB42 subsequently binds to the promoter of *NbPAL6*, enhancing its expression. NbPAL6 promotes SA biosynthesis, boosting SA-mediated defense against phloem-feeding insect whiteflies. The age-related rise in SA levels determines the ARR of plants. This model illustrates a seesaw-like mechanism for balancing growth and herbivore defense, with auxin dominance in early stages and SA-driven defense taking precedence as the plant ages.

Supplementary Materials

This PDF file includes:
Supplementary Text
Figs. S1 to S10
Other Supplementary Material for this manuscript includes the following:
Tables S1 to S2

Supplementary Figures

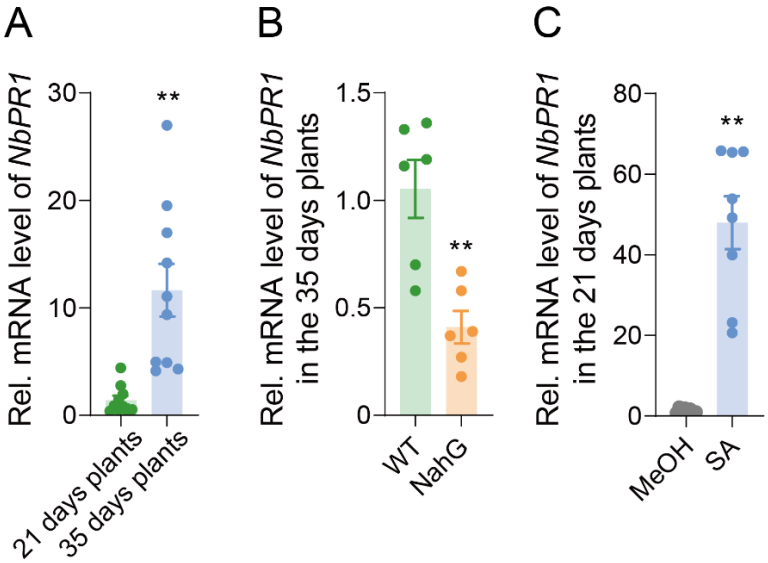

Fig. S1. Expression of the *NbPR1* gene downstream of SA at different ages and SA levels. (**A**) Expression level of the SA downstream gene *NbPR1* in the *N. benthamiana* plants at 21 and 35 days old. (**B**) Expression level of *NbPR1* in 35-day-old NahG *N. benthamiana* plant. (**C**) Expression level of *NbPR1* in 21-day-old *N. benthamiana* plants treated with 1 mM SA. Values are mean ± SE, $n = 10$ for **A** $n = 6$ for **B**; $n = 8$ for **C**. Student's *t*-test (two-tailed) was used for significant difference analysis. $^{**}P < 0.01$.

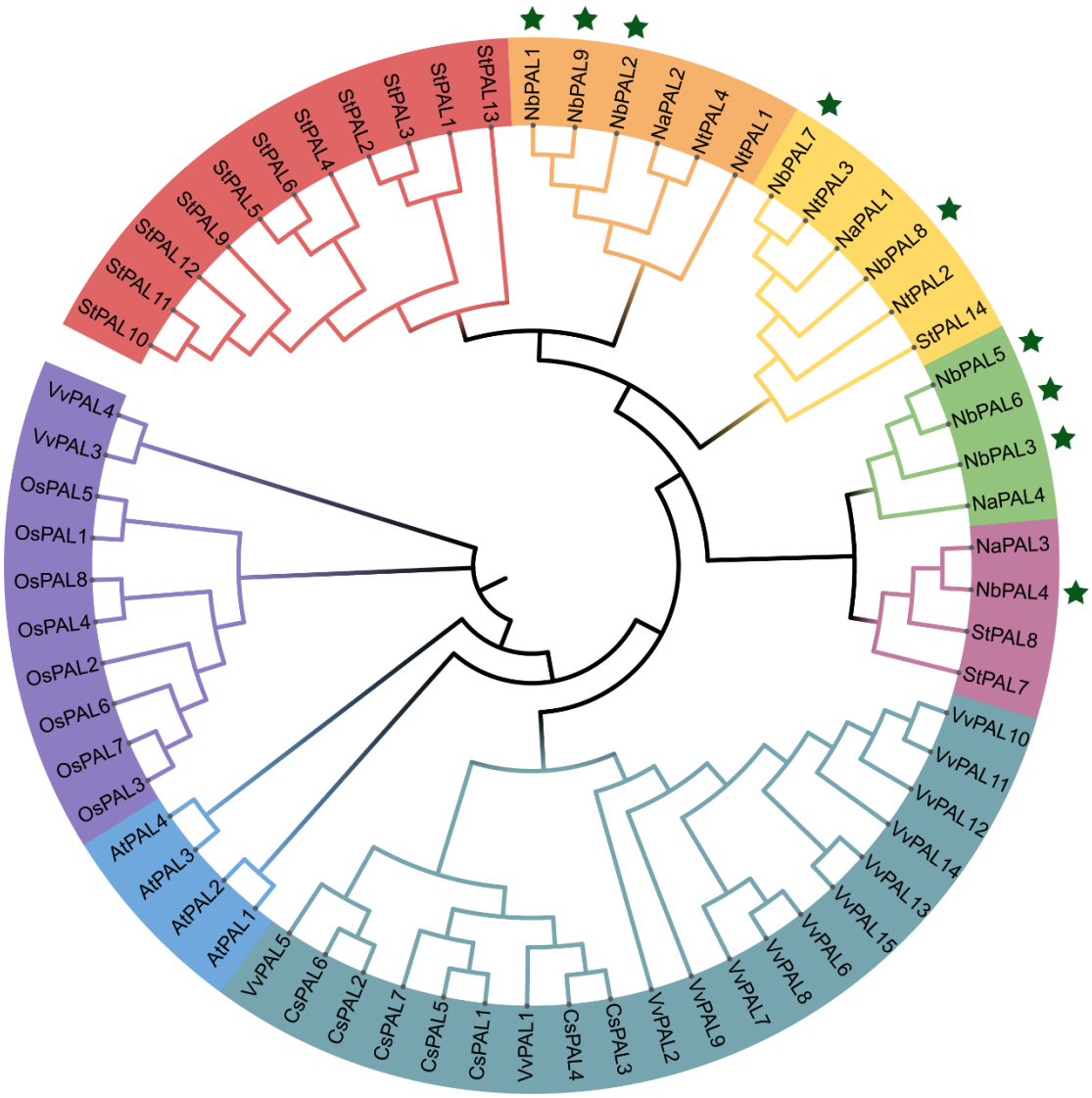

Fig. S2. Phylogenetic tree of PAL protein. Amino acid sequences of PAL proteins from *N. benthamiana* (Nb), *N. tabacum* (Nt), *N. attenuata* (Na), *Arabidopsis thaliana* (At), *Oryza sativa* (Os), *Solanum tuberosum* (St), *Vitis vinifera* (Vv), and *Camellia sinensis* (Cs) were aligned by ClustalW. The Maximum Likelihood tree was constructed with MEGA X with 1000 bootstrap replicates.

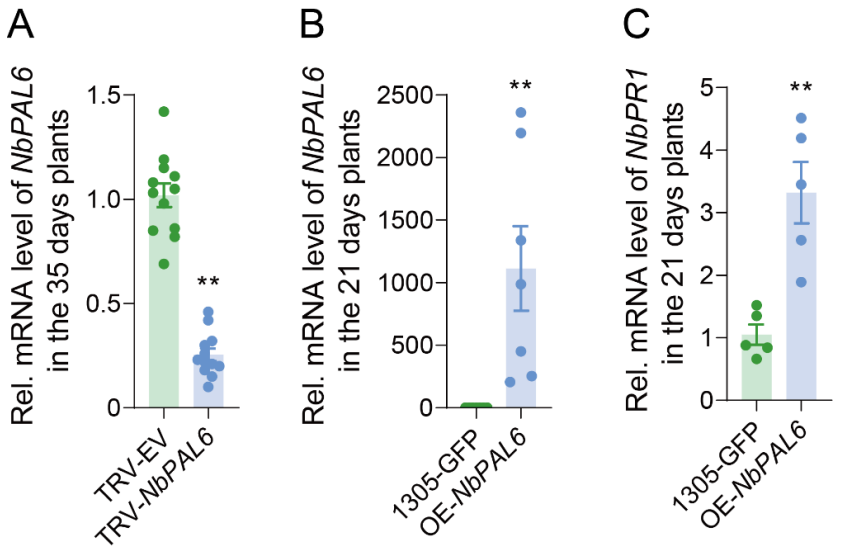

Fig. S3. Gene expression level after silencing and overexpressing *NbPAL6*. (**A**) Expression level of *NbPAL6* in *NbPAL6*-silenced 35-day-old *N. benthamiana* plants. (**B**) Expression level of *NbPAL6* in *NbPAL6*-overexpressed 21-day-old *N. benthamiana* plants. (**C**) Expression level of SA downstream *NbPR1* gene in *NbPAL6*-overexpressed 21-day-old *N. benthamiana* plants. Values are mean ± SE, $n = 12$ for **A** $n = 7$ for **B**; $n = 5$ for **C**. Student's *t*-test (two-tailed) was used for significant difference analysis. $^{**}P < 0.01$.

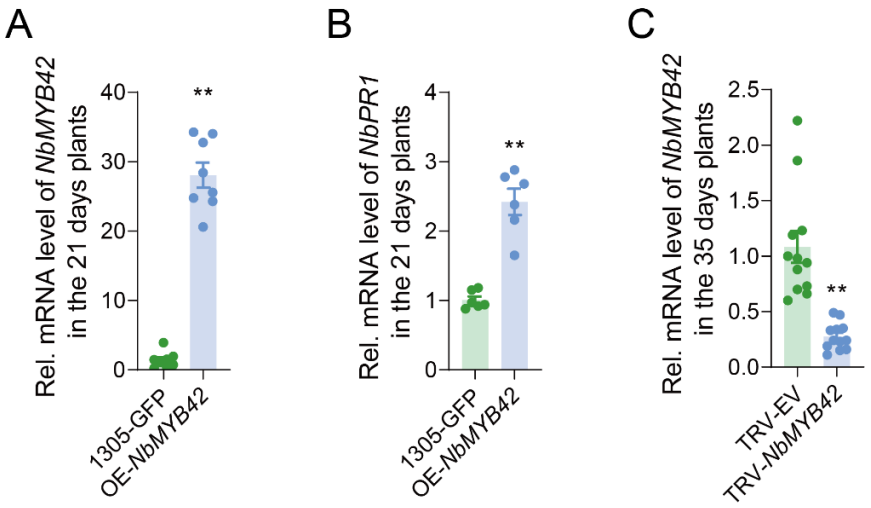

Fig. S4. Gene expression level after silencing and overexpressing *NbMYB42*. (**A**) Expression level of *NbMYB42* in the *NbMYB42*-overexpressed 21-day-old *N. benthamiana* plants. (**B**) Expression level of SA downstream *NbPR1* gene in the *NbMYB42*-overexpressed 21-day-old *N. benthamiana* plants. (**C**) Expression level of *NbMYB42* in *NbMYB42*-silenced 35-day-old *N. benthamiana* plants. Values are mean ± SE, $n = 8$ for **A**; $n = 6$ for **B**; $n = 12$ for **C**. Student's *t*-test (two-tailed) was used for significant difference analysis. $^{**}P < 0.01$.

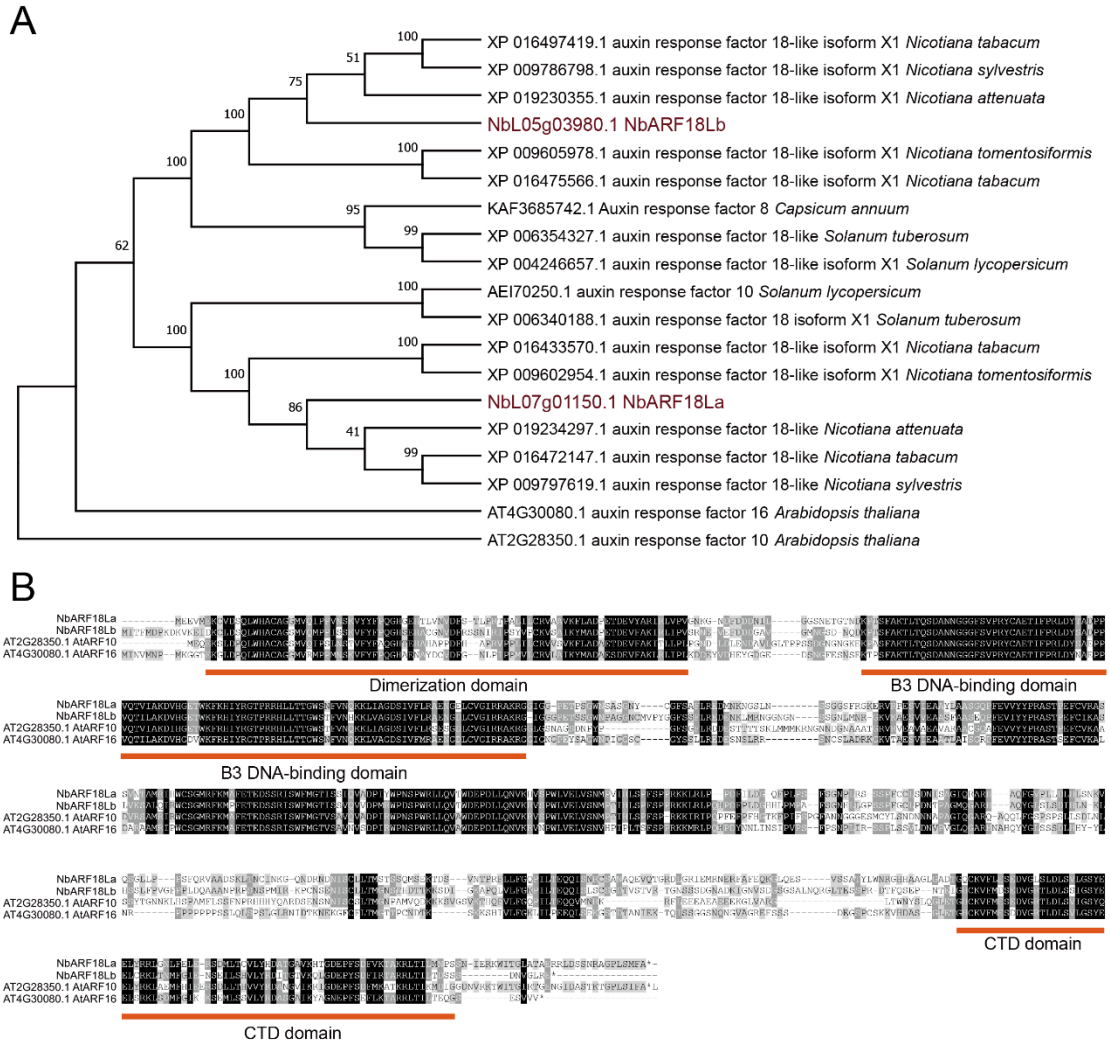

Fig. S5. Phylogenetic relationship and conserved DNA binding domain of NbARF18La/b. (**A**) Phylogenetic tree of ARF proteins. Homologous genes of NbARF18Ls were identified using NCBI Blast (https://blast.ncbi.nlm.nih.gov/Blast.cgi). Protein sequences were aligned using ClustalW, and a phylogenetic tree with 1000 bootstrap replicates was constructed by the Maximum Likelihood method in MEGA X. (**B**) Multi-sequence alignment analysis of ARF proteins. The B3 DNA binding domain (DBD) and C-terminal dimerization domain (CTD) regions are underlined. Protein sequence alignment results were visualized by GenDoc.

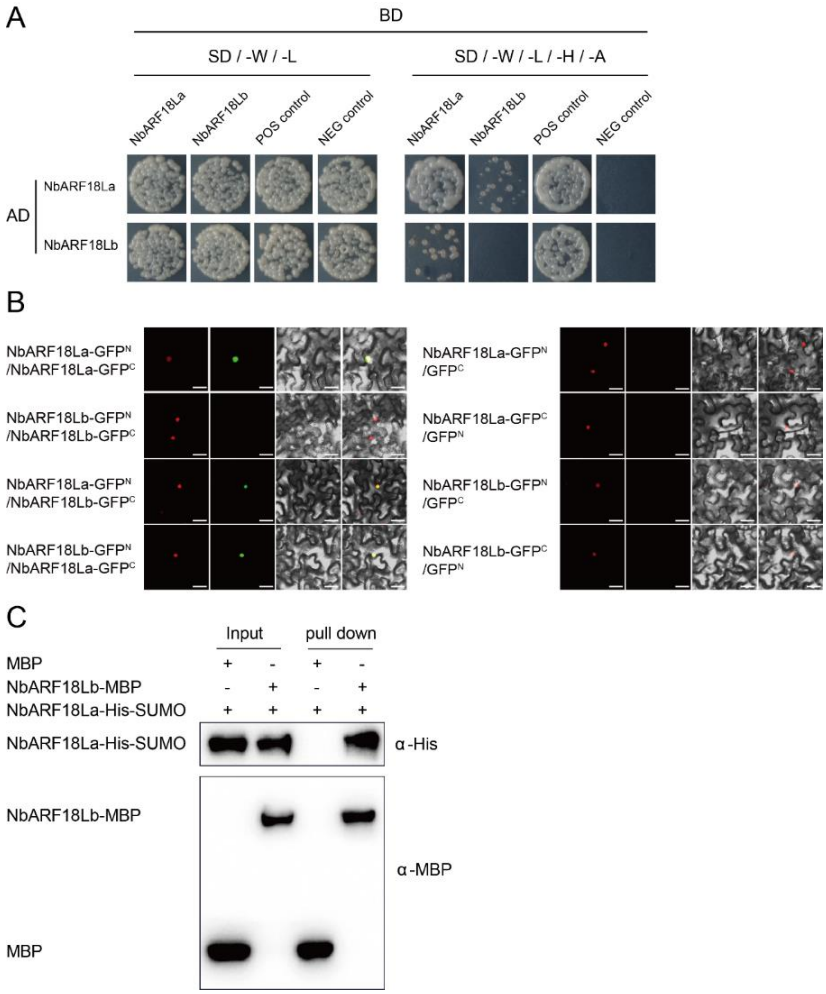

Fig. S6. NbARF18La interacts with NbARF18Lb. (**A**) Yeast two-hybrid (Y2H) assay between NbARF18La and NbARF18Lb. Yeast cells co-transformed with NbARF18La and NbARF18Lb plasmids grow on a selective medium (SD/-W-L-H-A) for 3 days, indicating an interaction between NbARF18La and NbARF18Lb. Additionally, yeast cells co-transformed with NbARF18La plasmids (pGADT7-NbARF18La and pGBKT7-NbARF18La) also grew on selective medium (SD/-W-L-H-A), showing that NbARF18La exhibits self-interaction. (**B**) Bimolecular fluorescence complementation (BiFC) assays confirmed the interaction between NbARF18La and NbARF18Lb in *N. benthamiana* epidermal cells. BiFC assays show that NbARF18La interacts with NbARF18Lb in nuclei, and NbARF18La interacts with itself in nuclei. The BiFC signal (green fluorescence) observed in the nuclei indicates an interaction between NbARF18La and NbARF18Lb, as well as a self-interaction of NbARF18La. Confocal microscopy was used to visualize the fluorescence. Scale bars, 40 μm. (**C**) The interaction between NbARF18La and NbARF18Lb was further validated by an *in vitro* pull-down assay. Recombinant NbARF18Lb-MBP and NbARF18La-His-SUMO proteins were incubated with MBP beads in a pull-down binding buffer. The pulled-down proteins were detected by immunoblotting using anti-MBP and anti-His antibodies. A mixture of MBP and NbARF18La-His-SUMO was used as a negative control.

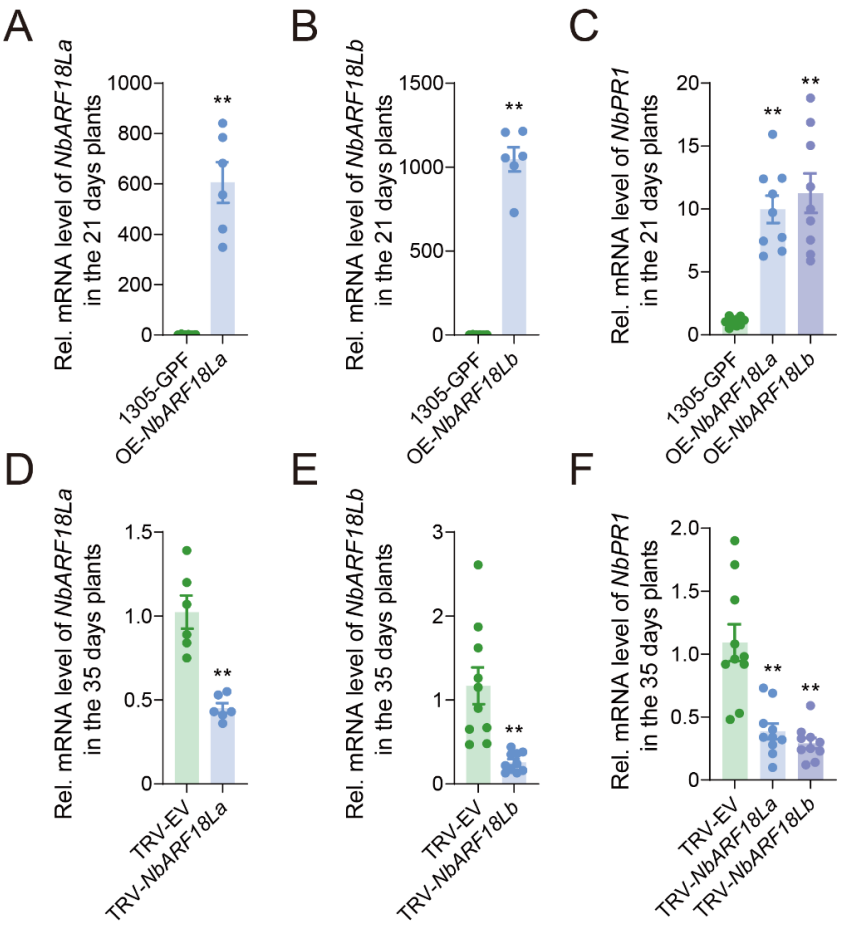

Fig. S7. Gene expression levels after overexpressing and silencing *NbARF18La/b*. (**A**, **B**) Expression levels of *NbARF18La*/*b* in the *NbARF18La*/*b*-overexpressed 21-day-old *N. benthamiana* plants. (**C**) Expression level of SA downstream gene *NbPR1* in the *NbARF18La*/*b*-overexpressed 21-day-old *N. benthamiana* plants. (**D**, **E**) Expression levels of *NbARF18La* and *NbARF18Lb* in the *NbARF18La*/*b*-silenced 35-day-old *N. benthamiana* plants. (**F**) Expression level of SA downstream gene *NbPR1* in the *NbARF18La*/*b*-silenced 35-day-old *N. benthamiana* plants. Values are mean ± SE, $n = 6$ for **A**, **B** and **D**; $n = 9$ for **C**; $n = 10$ for **E** and **F**. Student's *t*-test (two-tailed) was used for significant difference analysis. $^{**}P < 0.01$.

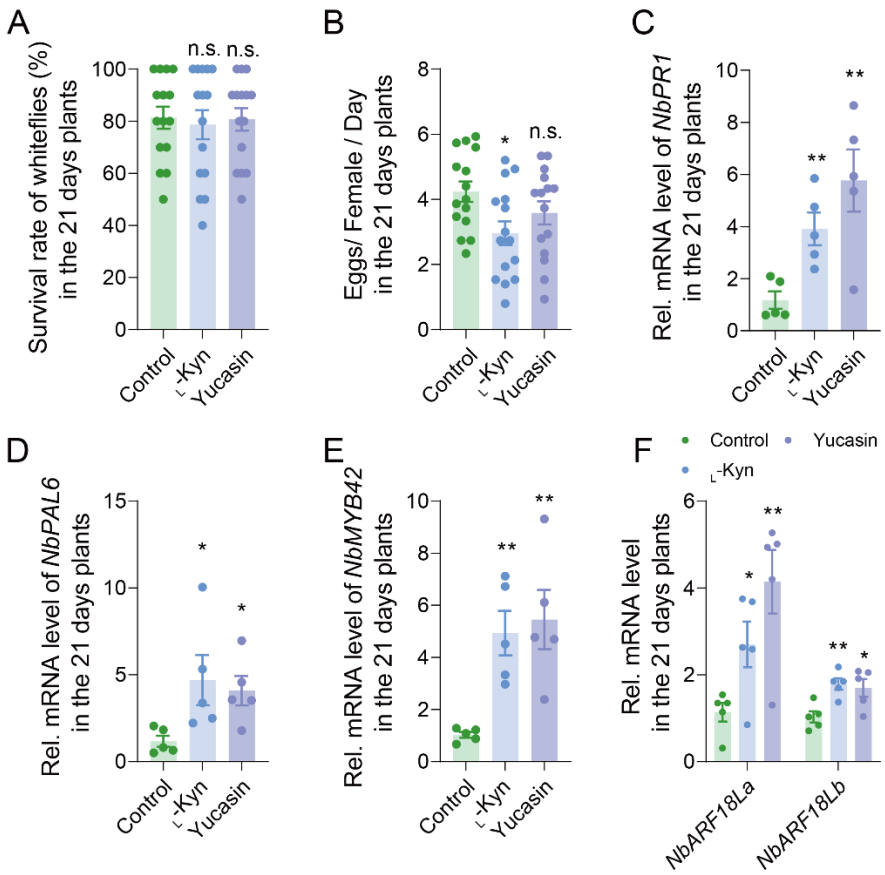

Fig. S8. Auxin synthesis inhibitors enhance the NbARF18La/b-MYB42 module in juvenile plants. (**A**) Survival rate and fecundity of whiteflies on *N. benthamiana* plants treated with L-Kyn and Yucasin (50 μM) at 21 days old. (**B**) SA levels in *N. benthamiana* plants treated with the IAA inhibitors L-Kyn and Yucasin (50 μM) at 21 days old. (**C**) Expression level of SA downstream gene *NbPR1* in L-Kyn- and Yucasin-treated (50 μM) 21-day-old *N. benthamiana* plants. (**D**) Expression level of *NbPAL6* in L-Kyn- and Yucasin-treated (50 μM) 21-day-old *N. benthamiana* plants. (**E**) Expression level of *NbMYB42* in L-Kyn- and Yucasin-treated (50 μM) 21-day-old *N. benthamiana* plants. (**F**) Expression levels of *NbARF18La/b* in the L-Kyn- and Yucasin-treated (50 μM) 21-day-old *N. benthamiana* plant. Values are mean ± SE, n = 15 for **A** and **B**; n = 5 for **C**, **D**, **E**, and **F**. Student's t-test (two-tailed) was used for significant difference analysis. n.s., not significant; *$P < 0.05$, **$P < 0.01$.

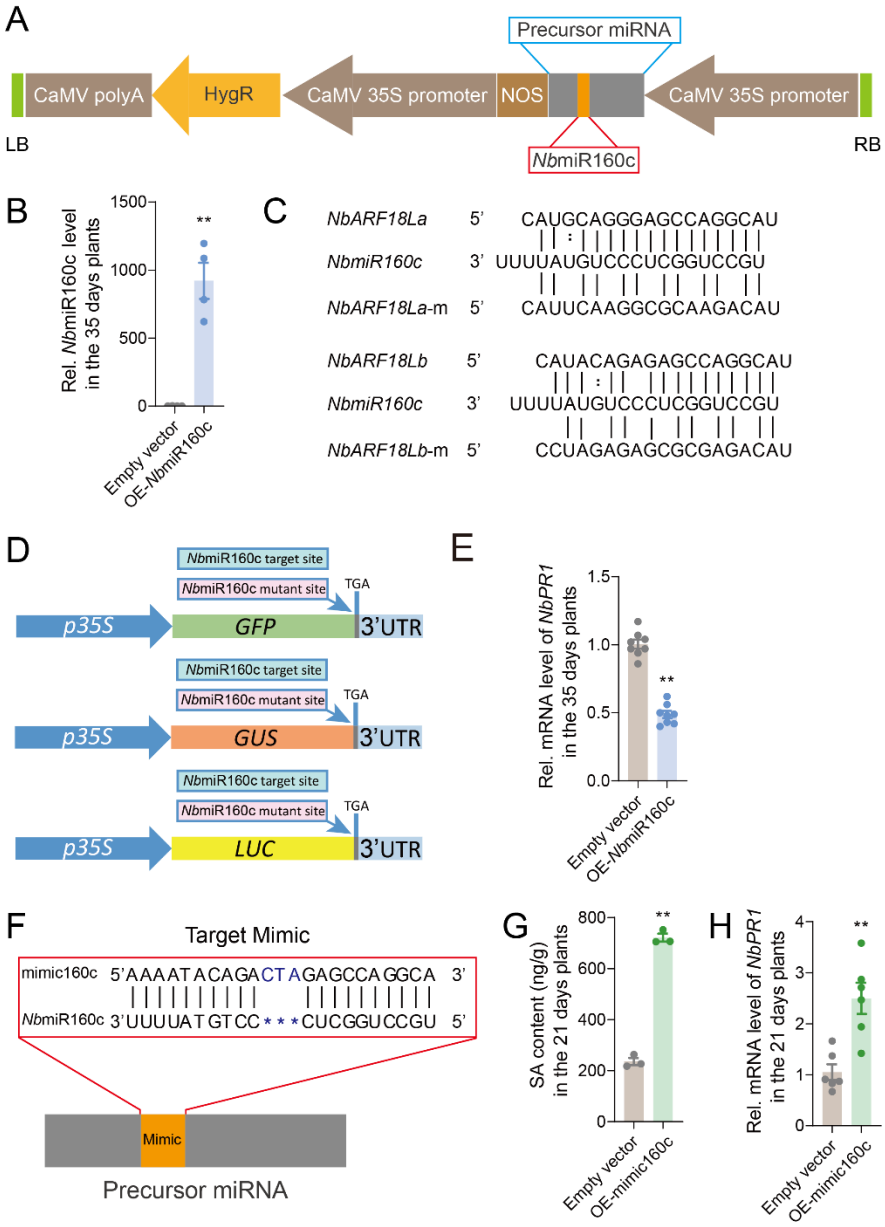

Fig. S9. Overexpression of mimicRNA160c increased the salicylic acid level in juvenile plants. (**A**) Schematic diagram of the *Nb*miR160c expression cassette *p35S-Nb*miR160c. This vector was used to overexpress *Nb*miR160c in *N. benthamiana* plants through *Agrobacterium*-mediated transformation. The blue box represents the miRNA precursor, and the red box represents *Nb*miR160c. HygR: Hygromycin B phosphotransferase; NOS: Nos Terminator; RB: Right border; LB: Left border. (**B**) Expression level of *Nb*miR160c in the *Nb*miR160c-expressed 35-day-old plants. (**C**) Sequence alignment of *Nb*miR160c with the predicted target sites in *NbARF18La* and *NbARF18Lb*, along with their mutated versions (*NbARF18La*-m and *NbARF18Lb*-m) used in subsequent experiments. Colons represent G: U pairs. (**D**) Schematic diagram of the GFP/GUS/LUC sensor carrying the *Nb*miR160c target site and the mutant target site. TGA: Termination codon; UTR: Untranslated regions. (**E**) Expression level of SA downstream gene *NbPR1* in the *Nb*miR160c-expressed 35-day-old plants. (**F**)

1562 Design of mimicry sequences (mimic160c) for *Nb*miR160c. (**G**) SA levels in
1563 mimic160c-expressed 21-day-old plants. (**H**) Expression level of SA downstream
1564 gene *NbPR1* in the mimic160c-expressed 21-day-old plants. Values are mean ± SE, n
1565 = 4 for **B**; n = 8 for **E**; n = 3 for **G**; n = 6 for **H**. Student's t-test (two-tailed) was used
1566 for significant difference analysis. $^{**}P < 0.01$.

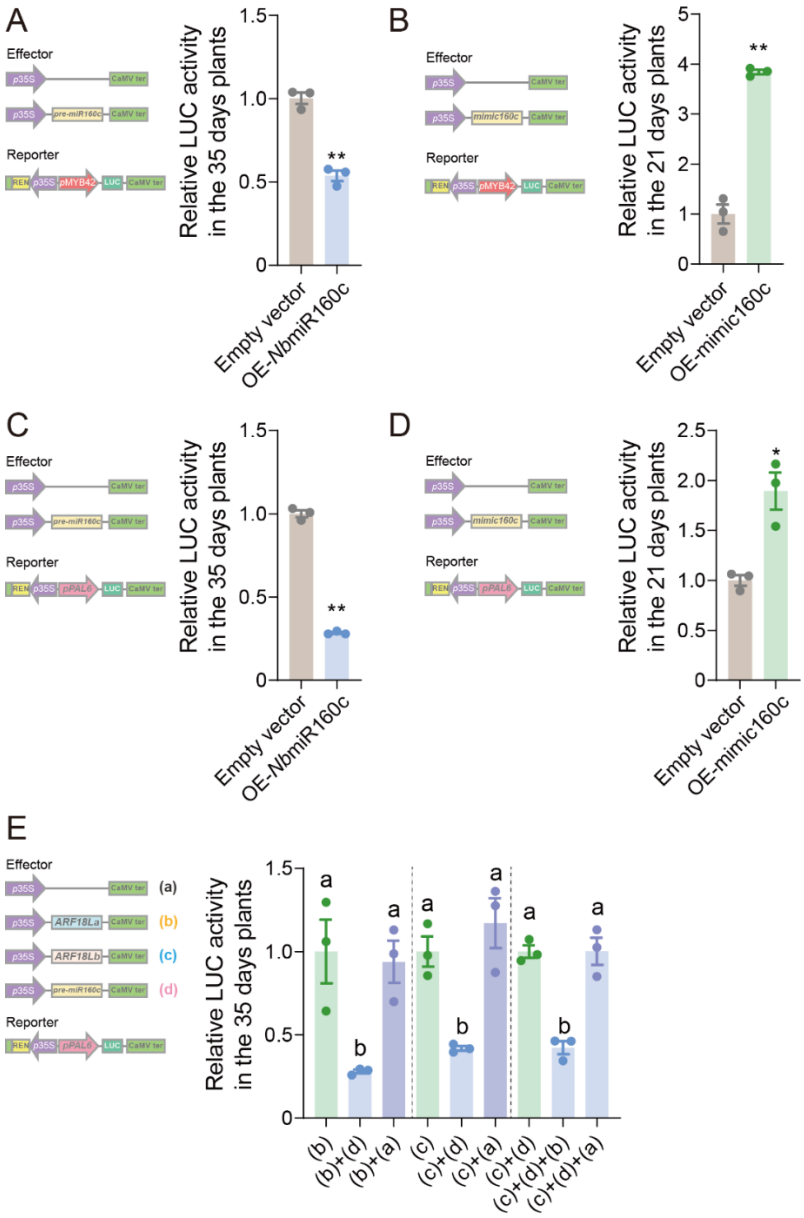

Fig. S10. *Nb*miR160c affects the transcription of *NbMYB42* and *NbPAL6*. (**A** to **E**) Schematic diagram showing the effector and reporter vectors used in transient transcriptional activity assays in *N. benthamiana* leaves. The data show the relative LUC activity normalized to REN activity. Values are mean ± SE, $n = 3$. Student's *t*-test (two-tailed) was used for significant difference analysis in **A**, **B**, **C**, and **D**. $*P < 0.05$, $**P < 0.01$. One-way ANOVA followed by Fisher's least significant difference (LSD) test was used for significant difference analysis in **E**. Bars with different lowercase letters indicate significant differences between treatments at $P < 0.05$.

Supplementary Tables

Table S1. Basic information on identifying *NbPAL* genes.

Gene Name	Gene ID	CDS (bp)	Protein Length (aa)	Molecular Weight (Da)
NbPAL1	NbL01g24700.1	2040	679	73888.46
NbPAL2	NbL05g03880.1	2154	717	78005.01
NbPAL3	NbL10g04670.1	2154	717	78248.28
NbPAL4	NbL10g08440.1	2166	721	78734.94
NbPAL5	NbL12g19650.1	2154	717	78393.48
NbPAL6	NbL13g11330.1	2154	717	78233.31
NbPAL7	NbL14g10160.1	2139	712	77447.38
NbPAL8	NbL15g02170.1	2139	712	77438.39
NbPAL9	NbL15g24630.1	2154	717	78151.22

1579 **Table S2.** List of primers used in this study.

Primer name	Sequence (5’-3’)
q-mir160c-F	TGCCTGGCTCCCTGTATTTT
q-NbU6-F	GGAACGATACAGAGAAGATTAGCA
q-NbACTIN-F	CAATCCAGACACTGTACTTTCTCTC
q-NbACTIN-R	AAGCTGCAGGTATCCATGAGACTA
q-NbPR1-F	TGCAAATCAGAGAGCTGGGG
q-NbPR1-R	CACTTTTCCCGGTGCACAAG
q-NbICS1-F	CGTGCTTATGGGGCAATTCG
q-NbICS1-R	ATTGCCATCTGGTACGTGCA
q-NbICS2-F	CTCGCGAGTACTCATGTCCC
q-NbICS2-R	ATCAATGTCCGCAGCTGTCA
q-NbEPS1-F	GCCGGCGTAGAATTCACCTA
q-NbEPS1-R	GCCGACGTTATTGAGTGGGA
q-NbCBP60g-F	CGACCTTGGCAAGCAGTTTC
q-NbCBP60g-R	GGAGAAACTGGCTGGATGCT
q-NbSARD1-F	AGTTGGCCACTGTTGACACA
q-NbSARD1-R	AGTGTAGTTTGCTCCGGTGG
q-NbEDS5-F	CAAACACTGCTGCTGCACAT
q-NbEDS5-R	AGGGACTTCAGCAACATCCG
q-NbPBS3-F	AACCCCGAAATTACCGACCC
q-NbPBS3-R	AGCACCCGTGACAATTACGT
q-NbEPS1-F	GCCGGCGTAGAATTCACCTA
q-NbEPS1-R	GCCGACGTTATTGAGTGGGA
q-NbMYB42-F	GGTGAGAGCTCCTTGTTGTGA
q-NbMYB42-R	TCTCCAATTGCCATGGCCAT
q-NbPAL4-F	ATGCACTCAAGGGTAGCCAC
q-NbPAL4-R	CAGCTCCACCATCACCTCTG
q-NbPAL6-F	AGGAACAAGGCATTGCATGG
q-NbPAL6-R	TTTCCAATGGAGGCAAGTGC
q-NbPAL7-F	ACAATCAGGGACAAGGGCAG
q-NbPAL7-R	GACCTGTGAGTAAACCGGCA
q-NbPAL9-F	TGTTTACCTCTCCGTGGCAC
q-NbPAL9-R	CAGCATTAAGGGCCTCACCA
q-NbARF18La-R	TGATCCCATCTACTGGCCCA
q-NbARF18La-F	GAGACCAGTTCGACAAGCCA
q-NbARF18Lb-F	CAACTCGTGCTTTTCGGCAA
q-NbARF18Lb-R	AGTGCAGAACCTGAGCCATC
q-NbTAR2-F	GCTGAGACTGGAAACCGACA
q-NbTAR2-R	CGAATAAAATGGGGCAGCGG
q-NbYUC8-F	GCAAATGGCGCTGAAGTTGA
q-NbYUC8-R	TGCCAGAATTTCCACAGCCA

Primer name	Sequence (5’-3’)
q-NbIAA29-F	CGTTTAAGGCTTGCGACGAG
q-NbIAA29-R	CCAATGGCCACTCCTTCCAT
pBI121-pNbPAL6-F	GACCATGATTACGCCAAGCTTGAATTCGTTCGGAAATTATGA
pBI121-pNbPAL6-R	ACCACCCGGGGATCCTCTAGAAAATGGAAAATATGAAAGAAAAAGA
pBI121-pNbARF18La-F	GACCATGATTACGCCAAGCTTCGCATGCAATCAAATATTATTACTCT
pBI121-pNbARF18La-R	ACCACCCGGGGATCCTCTAGATTGCCTTATCCAGTACACTTCT
pBI121-pNbARF18Lb-F	GACCATGATTACGCCAAGCTTGAGGTGAGGATTGCCCAAGC
pBI121-pNbARF18Lb-R	GGACTGACCACCCGGGGATCCCTTGATTTCAACAGAATTTTACAGA
pBI121-pNbMYB42-F	GCTATGACCATGATTACGCCAAGCTTTAGTGATTTGACTGTGCGTGA
pBI121-pNbMYB42-R	GACTGACCACCCGGGGATCCTCTAGATTTTGCTTTAATCACTTGCT
pBI121-pmir160-F	AGCTATGACCATGATTACGCCAAGCTTAATTTGACTATTACATAATTCCT
pBI121-pmir160-R	GGACTGACCACCCGGGGATCCCGAGGAAAATACGAAGTGAA
TRV-NbARF18La-F	GCTCTAGAACCCAGTTTCCAGCGAGTTG
TRV-NbARF18La-R	CGGGATCCTCTTGAAGACCTTTCTGCTCA
TRV-NbARF18Lb-F	GCTCTAGAAATCCAGCTGGTGGGAACTG
TRV-NbARF18Lb-R	CGGGATCCAAAAGGCATCTTGAACCTCATCC
TRV-NbPAL6-F	GCTCTAGATCTATGGTTCTATTTGAGGCT
TRV-NbPAL6-R	CGGGATCCGGCCCTAATGACCTCAATTTGA
TRV-NbMYB42-F	GAGTAAGGTTACCGAATTCTCTAGAAAAGACACTCCAAAAACAATCTTGA
TRV-NbMYB42-R	GTGAGCTCGGTACCGGATCCTTGGTCATCGATTGTAATAGTCGT
1305-NbARF18La-F	TAAGTCCGGAGCTAGCTCTAGAATGGAGGAGGTTATGGAGAAATGT
1305-NbARF18La-R	CGGTCCTCGAGACGTCTCTAGATGCAAACATGCTAAGTGGTCC
1305-NbARF18Lb-F	TAAGTCCGGAGCTAGCTCTAGAATGATTACTTTTATGGATCCAAAGGAC
1305-NbARF18Lb-R	CGGTCCTCGAGACGTCTCTAGACTCCCTGAGTCCAACATTATCG
1305-NbPAL6-F	GCTCTAGAATGGAGTATGCAAATGGAGATTGT

Primer name	Sequence (5’-3’)
1305-NbPAL6-R	CGGGATCCGCAGAGTGGAAGAGGAGC
1305-NbMYB42-F	GCTCTAGAATGGTGAGAGCTCCTTGTTGT
1305-NbMYB42-R	CGGGATCCAAATTCCGGTAAATCTAGT
pABAi-pNbMYB42-F	AAAAAAAATGATGAATTGAAAAGCTTTAGTGATTTGACTGTGCGTGA
pABAi-pNbMYB42-R	TCGAGGTCGACAGATCCCCGGGTACCTTTTGCTTTAATCACTTGCT
pABAi-pNbPAL6-F	AAAAAAAATGATGAATTGAAAAGCTTGAATTCGTTCGGAAATTATGA
pABAi-pNbPAL6-R	TCGAGGTCGACAGATCCCCGGGTACCAAATGGAAAATATGAAAGAAAAAGA
pGAD-NbARF18La-F	CCGGGTGGGCATCGATACGGGATCCATGGAGGAGGTTATGGAGAAATGT
pGAD-NbARF18La-R	TATCTACGATTCATCTGCAGCTCGAGCTATGCAAACATGCTAAGTGGTCC
pGAD-NbARF18Lb-F	CCGGGTGGGCATCGATACGGGATCCATGATTACTTTTATGGATCCAAAGGAC
pGAD-NbARF18Lb-R	TATCTACGATTCATCTGCAGCTCGAGTTACTCCCTGAGTCCAACAT
pGAD-NbMYB42-F	CGGGATCCATGGTGAGAGCTCCTTGTTGT
pGAD-NbMYB42-R	CCCTCGAGTCAAAATTCCGGTAAATCTAGT
pGBK-NbARF18La-F	TGGCCATGGAGGCCGAATTCATGGAGGAGGTTATGGAGAAATGT
pGBK-NbARF18La-R	CGCTGCAGGTCGACGGATCCCTATGCAAACATGCTAAGTGGTCC
pGBK-NbARF18Lb-F	TGGCCATGGAGGCCGAATTCATGATTACTTTTATGGATCC
pGBK-NbARF18Lb-R	CGCTGCAGGTCGACGGATCCCTACTCCCTGAGTCCAACAT
pGreen0800-pNbPAL6-F	TCGAGGTCGACGGTATCGATAAGCTTGAATTCGTTCGGAAATTATGA
pGreen0800-pNbPAL6-R	GGCCGCTCTAGAACTAGTGGATCCAAATGGAAAATATGAAAGAAAAAGA
pGreen0800-pNbMYB42-F	TCGAGGTCGACGGTATCGATAAGCTTTAGTGATTTGACTGTGCGTGA
pGreen0800-pNbMYB42-R	GCGGCCGCTCTAGAACTAGTGGATCCTTTTGCTTTAATCACTTGCT
pGreen0800-pmir160-F	ACTCACTATAGGGCGAATTGGGTACCAATTTGACTATTACATAATTCCT
pGreen0800-pmir160-R	CGGCCGCTCTAGAACTAGTGGATCCCGAGGAAAATACGAAGTGAA
pET28a-SUMO-NbARF18La-F	GCTCACAGAGAACAGATTGGTGGAATGGAGGAGGTTATGGAGAAATGTG

Primer name	Sequence (5’-3’)
pET28a-SUMO-NbARF18La-R	TGCCGCCACTACCACCACCACTACCACCGCCTTTTTCAAACTGCGGATGGCTCCATGCAAACATGCTAAGTGGTCCTGC
pMAL-NbARF18Lb-F	TCCAGGGGCCCCTGGGATCCATGATTACTTTTATGGATCC
pMAL-NbARF18Lb-R	CTGCCGCCACTACCACCACCACTACCACCGCCTTTTTCAAACTGCGGATGGCTCCACTCCCTGAGTCCAACATTATCGC
pGEX-NbMYB42-F	CTGGAAGTTCTGTTCCAGGGGCCCGGCTCCATGGTGAGAGCTCCTTGTTGTGA
pGEX-NbMYB42-R	CACTACCACCACCACTACCACCGCCTTTTTCAAACTGCGGATGGCTCCAAAATTCCGGTAAATCTAGTAAGTCCCCG
1300-mir160-F	GGGGTACCCAGCAGCAGCCACAGCAAAA
1300-mir160-R	CGGGATCCGCTGCTGATGCTGATGCCAT
1300-mimic160-F	GGTACCTGGCCATCCCCTA
1300-mimic160-R	GGATCCCGGAAGCAAATTTACA
Bifc-NbARF18La-F	CCATTTACGAACGATAGTTAATTAACATGGAGGAGGTTATGGAGAAATGT
Bifc-NbARF18La-R	CCACCACTGCCACCTCCTCCACTAGTTGCAAACATGCTAAGTGGTCC
Bifc-NbARF18Lb-F	CCATTTACGAACGATAGTTAATTAACATGATTACTTTTATGGATCCAAAGGAC
Bifc-NbARF18Lb-R	CCACCACTGCCACCTCCTCCACTAGTCTCCCTGAGTCCAACATTATCG
35S-GFP-mir160-F	AGGACCGGTCCCGGGGGATCCATGGTGAGCAAGGGCGAG
GFP-NbARF18La-site-R	GGGCGGCCGCTTTAAGATCTATGCCTGGCTCTCTGTATGC
GFP-NbARF18La-mutant site-R	GGGCGGCCGCTTTAAGATCTATGTCTCGCGCTCTCTAGGC
GFP-NbARF18Lb-site-R	GGGCGGCCGCTTTAAGATCTATGCCTGGCTCCCTGCAT
GFP-NbARF18Lb-mutant site-R	GGGCGGCCGCTTTAAGATCTATGTCTTGCGCCTTGAATGC
35S-GUS-mir160-F	GGAGAGAACACGGGGGACTCTAGAATGTTACGTCCTGTAGAAACCCC
GUS-NbARF18La-site-R	AACGATCGGGGAAATTCGAGCTCTCAATGCCTGGCTCTCTGTATGCC
GUS-NbARF18La-mutant site-R	AACGATCGGGGAAATTCGAGCTCTCAATGTCTCGCGCTCTCTAGGCC
GUS-NbARF18Lb-site-R	AACGATCGGGGAAATTCGAGCTCTCAATGCCTGGCTCCCTGCATGCC
GUS-NbARF18Lb-mutant site-R	AACGATCGGGGAAATTCGAGCTCTCAATGTCTTGCGCCTTGAATGCC
35S-LUC-mir160-F	CATGCCATGGAAGACGCCAA
LUC-NbARF18La-site-R	GCTCTAGAATGCCTGGCTCTCTGTATGCCATTACACGGCGATCTTTCCG

Primer name	Sequence (5’-3’)
LUC-NbARF18La-mutant site-R	GCTCTAGAATGTCTCGCGCTCTCTAGGCCATTACACGGCGATCTTTCCG
LUC-NbARF18Lb-site-R	GCTCTAGAATGCCTGGCTCCCTGCATGCCATTACACGGCGATCTTTCCG
LUC-NbARF18Lb-mutant site-R	GCTCTAGAATGTCTTGCGCCTTGAATGCCATTACACGGCGATCTTTCCG
ChIP-pNbMYB42-P1-F	AGTGATTTGACTGTGCGTGA
ChIP-pNbMYB42-P1-R	AAAACGGCACAAATGGTCCG
ChIP-pNbMYB42-P2-F	AACTTGAGAACCCACGACCC
ChIP-pNbMYB42-P2-R	CCTGCATGGAAATTCATGAAATCT
ChIP-pNbMYB42-P3-F	ACTCCTTCAGATTTTGACGTGA
ChIP-pNbMYB42-P3-R	ACCTTATTTACGAGGATTACACTGAGT
ChIP-pNbPAL6-P1-F	TCGGTCTCAACGCGTTAATGA
ChIP-pNbPAL6-P1-R	ACTTTCCCTTCACCAACATGA
ChIP-pNbPAL6-P2-F	ATGACGTGGTGCTGTCGTTG
ChIP-pNbPAL6-P2-R	TTTCCCTCGTAAAATACCGCA
ChIP-pNbPAL6-P3-F	CGCCAGTAAGTTATTATCGCGC
ChIP-pNbPAL6-P3-R	CGTTGGATTGCACATGGAGA
ChIP-pNbPAL6-P4-F	TCTCCATGTGCAATCCAACG
ChIP-pNbPAL6-P4-R	TGTTGAGCCAAAATGTGAGTGT
ChIP-pNbPAL6-P5-F	TGGCTCAACAAACTCAGGAAATT
ChIP-pNbPAL6-P5-R	AATGTGTGTTGCGAACTTCTC
EMSA-pPAL6-F	GTGAGGGTTGAAGGGTGGTTGTTGAGAGGAAGCCCGCTTACTTTTTTTGG
EMSA-pPAL6-R	GGTTTTTTTCATTCGCCCGAAGGAGAGTTGTTGGTGGGAAGTTGGGAGTG
EMSA-pPAL6-mF	GTGAGGGTTGAAGAAAAAAAAAAAAAAAAAAGCCCGCTTACTTTTTTTGG
EMSA-pPAL6-mR	GGTTTTTTTCATTCGCCCGAAAAAAAAAAAAAAAAAAGAAGTTGGGAGTG
EMSA-pMYB42-F	GGACAATTTTTCTTTATTTTCTTTTTTGTCTCCAGTAAAATAACG
EMSA-pMYB42-R	GCAATAAAATGACCTCTGTTTTTTCTTTTATTTCTTTTTAACAGG
EMSA-pMYB42-mF	GGACAATTTTTCTTTATTTTCTTTTTAAAAAACAGTAAAATAACG
EMSA-pMYB42-mR	GCAATAAAATGACAAAAAATTTTTCTTTTATTTCTTTTTAACAGG

1580